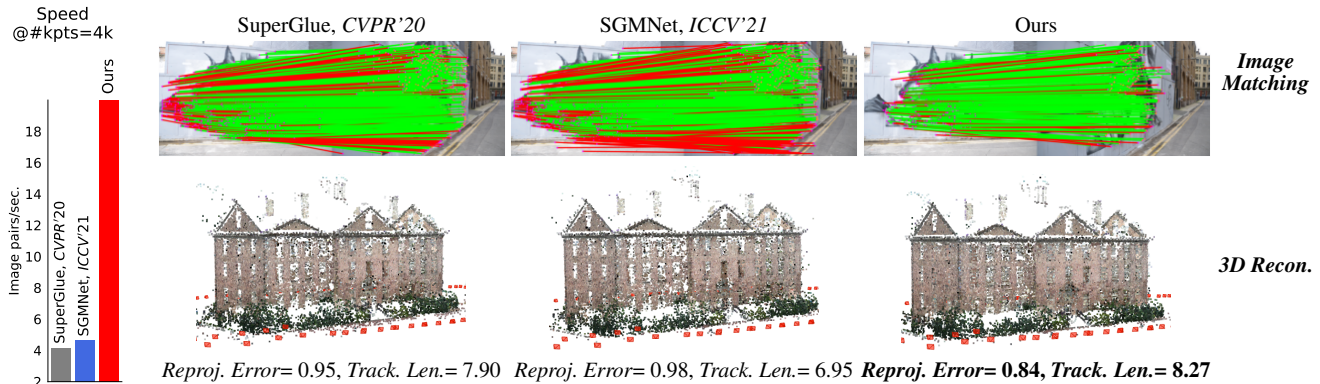


# Efficient Linear Attention for Fast and Accurate Keypoint Matching

Suwichaya Suwanwimolkul  
KDDI Research, Inc.  
Japan  
xsu-suwanui@kddi.com

Satoshi Komorita  
KDDI Research, Inc.  
Japan  
sa-komorita@kddi.com



**Figure 1: Our method versus the bigger SOTAs—SuperGlue and SGMNet—on speed (left), image matching\* (top), and 3D reconstruction (bottom).**

## Abstract

Recently Transformers have provided state-of-the-art performance in *sparse* matching, crucial to realize high-performance 3D vision applications. Yet, these Transformers lack efficiency due to the quadratic computational complexity of their attention mechanism. To solve this problem, we employ an efficient linear attention for the linear computational complexity. Then, we propose a new attentional aggregation that achieves high accuracy by aggregating both the global and local information from sparse keypoints. To further improve the efficiency, we propose the joint learning of feature matching and description. Our learning enables simpler and faster matching than Sinkhorn, often used in matching the learned descriptors from Transformers. Our method achieves competitive performance with only 0.84M learnable parameters against the bigger SOTAs, SuperGlue (12M parameters) and SGMNet (30M parameters), on three benchmarks, HPatch, ETH, and Aachen Day-Night.

## CCS Concepts

• **Computing methodologies** → **Computer vision problems.**

## Keywords

Sparse matching, learning-based matching, visual localization, SfM.

Permission to make digital or hard copies of all or part of this work for personal or classroom use is granted without fee provided that copies are not made or distributed for profit or commercial advantage and that copies bear this notice and the full citation on the first page. Copyrights for components of this work owned by others than ACM must be honored. Abstracting with credit is permitted. To copy otherwise, or republish, to post on servers or to redistribute to lists, requires prior specific permission and/or a fee. Request permissions from [permissions@acm.org](mailto:permissions@acm.org).

ICMR '22, Accepted version, Newark, NJ, USA.

© 2022 Association for Computing Machinery.

ACM ISBN 978-1-4503-9238-9/22/06...\$15.00

<https://doi.org/10.1145/3512527.3531369>

## ACM Reference Format:

Suwichaya Suwanwimolkul and Satoshi Komorita. 2022. Efficient Linear Attention for Fast and Accurate Keypoint Matching. In *Proceedings of the 2022 International Conference on Multimedia Retrieval (ICMR '22)*, June 27–30, 2022, Newark, NJ, USA. ACM, New York, NY, USA, 18 pages. <https://doi.org/10.1145/3512527.3531369>

## 1 Introduction

Local feature matching is a fundamental step to achieve high performance in vision applications, such as visual localization [39], Structure from Motion (SfM) [41], and 3D reconstruction [17]. Classical local feature matching starts from extracting feature descriptors and keypoints that are robust against various transformations. The local feature matching relies both on the descriptive power of the descriptors and the geometrical consistency of keypoints. The similarity of descriptors is crucial in finding the nearest neighbors in feature space. Recent studies [22, 34, 36, 44, 55] focused on using deep learning techniques to boost the descriptive power of the descriptors. Transformers have become the core technology to realize state-of-the-art performance in *sparse* matching [5, 36]. Specifically, the Transformers originated from [49] were extended to learn the descriptiveness of sparse keypoints through *self-attention* and *cross-attention* [5, 36]. Self-attention encodes the descriptiveness by aggregating information within an image; cross-attention aggregates the information between the pair.

Nevertheless, the efficiency of these Transformers [5, 36, 49] remains a critical issue when the number of keypoints is large. The major cause of the lack of efficiency is the quadratic computational complexity of softmax attention in these Transformers. Although Chen, *et al.* [5] attempted to improve the complexity of [36] by using

\*In image matching, green & red lines indicate the correct and incorrect matches.

seeds to represent groups of keypoints in matching, the complexity remains quadratic in the number of seeds:  $O(N^2C)$  for  $N$  denoting the number of seeds (or keypoints) and  $C$  denoting feature dimensions. Nevertheless, another reason for the lack of efficiency is the descriptors matching after encoding by the Transformers. In order to match the encoded descriptors, the existing works [5, 36] formulate the learning as an optimal transport problem where Sinkhorn algorithm [9, 50] is used to match the descriptors. The computational cost of Sinkhorn, however, is very high. In matching  $10k$  keypoints, Sinkhorn increases the runtime by an order of magnitude of the inference runtime of the Transformer [5].

To address this problem, we resort to using the linear attention [18, 44] that offers linear computational complexity, *i.e.*,  $O(NC^2)$ . However, it offered a lower or comparable accuracy than the regular softmax attention [8]. Thus, we further improve the accuracy of the linear attention for sparse keypoint matching by proposing a new attentional aggregation, namely *pairwise neighborhood attention*, to aggregate the local information from the neighborhoods of candidate matches in addition to the global information from the self- and cross-attention. Despite the accuracy improvement, the resulting complexity is kept low. Table 1 provides the time complexity of our proposed attention versus the SOTAs. To further improve the efficiency, we propose the joint learning of the description and sparse keypoint matching based on minimizing the feature distance. With the proposed learning, we can employ the feature distance-based matching such as [26], which is simpler and faster than Sinkhorn. Then, the performance can be improved further with efficient filtering based on the feature distance [4]. This results in competitive performance with a low computational cost against the existing SOTAs, as shown in Fig. 1. Our contributions are:

- Pairwise neighborhood attention to boost the performance of existing linear attention.
- Joint learning of the sparse keypoint matching and description via minimizing feature distance, which improves the feature description and enables the efficient matching and filtering.
- Competitive performance while having only  $0.84M$  learnable parameters, against the bigger SOTAs: SuperGlue [36] ( $12M$  parameters) and SGMNet [5] ( $30M$  parameters) on the benchmarks: HPatch, ETH, Aachen Day-Night.

## 2 Related works

### 2.1 Learnable local feature matching

**Sparse matching** has recently gained a large improvement over the local feature detection by learning to match the detected keypoints. Notably, SuperGlue [36] employed a Transformer similar to [49] to exchange both visual and geometric information between the pair of images. Nevertheless, the Transformer has quadratic computational complexity in the number of keypoints. Recently SGMNet [5] achieves the lower complexity by projecting  $N$  keypoints into  $K$  seeds. However, SGMNet still employs the softmax attention to aggregate the messages from seeds, which still results in, yet, a quadratic complexity  $O(NKC + K^2C)$ .

**Dense matching** [22, 33, 34, 44, 55] aims to match descriptors in a pixel-wise manner. To enumerate all the possible matches, the

**Table 1: Time complexity of our proposed attention vs. SOTAs'**

Methods	Comp. Complex.	Attention Type
SuperGlue [36]	$O(N^2C)$	Softmax attention [10, 49]
SGMNet [5]	$O(NKC + K^2C)$	Seeding + Softmax attention [5, 49]
Ours	$O(NC^2 + N_{max}C'^2)$ $\approx O(NC^2)$	Linear Attention Eq. (4) [18] + Pairwise Neighborhood Attention Eq. (5)

$N$  denotes the number of keypoints;  $C$  or  $C'$  denotes the associated feature dimensions after linear projection;  $K$  denotes the number of seeds in [5];  $N_{max}$  denotes the size of the largest neighborhood,  $N_{max} \ll N$ .

works [22, 33, 34] employed 4D cost volumes. Patch2Pix [55] took a step further from SparseNCNet [34] with an end-to-end learnable matching and refinement by regressing on pixel-level matches of local patches. Meanwhile, LoFTR [44] employed a ResNet with linear Transformer [18] for detector-less matching. Nevertheless, LoFTR matches every pixel between two images, leading to the large input's sequence length, *i.e.*,  $H_1 \times W_1$  (or  $H_2 \times W_2$ ), for  $H_1$  ( $H_2$ ) and  $W_1$  ( $W_2$ ) denoting the height and width of the image, which requires a much higher time and memory cost than the sparse matching.

### 2.2 Graph matching

Graph matching aims to establish node-to-node correspondences between two or multiple graphs, which are found in various applications [1, 6, 46–48]. Graph matching can be formulated as a Quadratic Assignment Problem (QAP) known to be NP-hard [25, 28]. Early works [15, 16, 21, 21, 45] improved the feasibility of QAP solvers. Recent works [13, 35, 53] leverage the graph matching with deep learning, yet they become less feasible in handling more than hundreds of keypoints [36]. Alternatively, the matching problem can be formulated as the optimal transport problem [50] where the Sinkhorn algorithm can be used to efficiently find the solution [9, 20, 30]. A recent study [9] improved the algorithm to achieve the nearly linear runtime of  $O(N^2/\epsilon^3)$ , where  $\epsilon$  is an error tolerance bound. However, Sinkhorn still requires an extreme runtime cost in matching thousands of keypoints or more, as evidenced by [5, 36].

### 2.3 Efficient Attention with Linear Complexity

Regular Transformers [10, 49] contain the powerful softmax attention. However, the softmax attention has the time complexity and memory scale quadratically with the input sequence length  $N$ , *i.e.*,  $O(N^2 \max(D, C))$  for  $D$  and  $C$  being the feature dimension of query and key. To solve this, Linear Transformers [18, 43, 51] reduce the computational cost to the linear complexity  $O(NDC)$  by computing the attention from the feature maps of dimensionality  $C$ , instead of the softmax attention. The feature maps offer lower or comparable accuracy than the softmax attention in applications such as speech recognition and image generation [8, 18]; however, it can approximate well *without imposing any constraints*, which is opposed to the previously developed techniques, *e.g.*, restricting attention [29], employing sparsity prior [7], pooling-based compression [31]. Others reduced the space complexity by sharing attention weights [19] or allowing one-time activation storage in training [7]. However, these approximations are not sufficient for long-sequence problems.

Our work is inspired by the Linear Transformers such as [18, 43, 51] that offer high efficiency. Meanwhile, the existing sparse



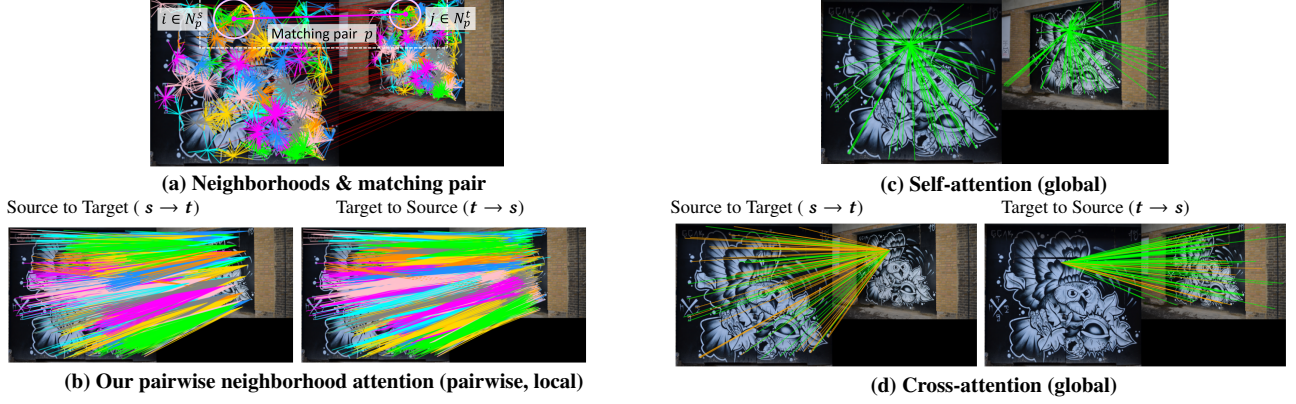


**Figure 2: Visualization of our pairwise neighborhood attention vs. self- and cross-attention. Given (a) sets of neighborhoods & matching pairs, one can aggregate information with (b) our pairwise neighborhood attention to collect the pairwise, local neighborhood information. Meanwhile, (c) self-attention and (d) cross-attention focus more on the global information within and between images.**

matching, *i.e.*, SuperGlue [36] and SGMNet [5] employ the regular Transformer [10, 49] with quadratic computational complexity. LoFTR [44] also uses Linear Transformer, but for dense matching to match every pixel, which offers the denser and more accurate matches. However, these matches are not suitable for large-scale 3D reconstruction due to the high computational cost caused by the redundant matches [24].

### 3 Proposed method

Our main proposal is the efficient Linear Transformer for *sparse matching*, where we employ two different types of attentional aggregation to collect the global and local information. Self- and cross-attention are used to aggregate the global information. Then, our proposed pairwise neighborhood attention is used to aggregate the local information. The visualization of the two attention is in Fig. 2. The formulation of our problem is first discussed. Then, we present the proposed Transformer, where we used a local neighborhood selection to extract the local information. Then, we match the extracted features with distance-based matching and filtering in matching. Finally, we confirm our design choice with the time complexity.

#### 3.1 Formulation

We consider the problem of finding the matched pairs between  $N$  and  $M$  keypoints in source and target images,  $I^s$  and  $I^t$ . Let  $\mathbf{k}^s, \mathbf{k}^t \in \mathcal{R}_+^{2 \times 2}$  denotes the sets of keypoint locations in the 2D images. Our goal is to encode the associated descriptors  $\mathbf{x}^s \in \mathcal{R}^{N \times D}, \mathbf{x}^t \in \mathcal{R}^{M \times D}$  via a parametric function  $\mathcal{F}_\Phi(\cdot)$  into new feature space such that it establishes the correct matching. This is formulated as finding the best set of parameters  $\Phi$  for the function  $\mathcal{F}_\Phi(\cdot)$  via minimizing:

$$\mathcal{L}_{triplet} = \frac{1}{|\mathcal{M}_+|} \sum_{c \in \mathcal{M}_+} s_c \cdot \mathcal{R}(\hat{\mathbf{x}}_c^s, \hat{\mathbf{x}}_c^t) \quad (1)$$

where  $\hat{\mathbf{x}}^s, \hat{\mathbf{x}}^t = \mathcal{F}_\Phi(\mathbf{x}^s, \mathbf{x}^t | \mathbf{k}^s, \mathbf{k}^t)$  and  $\mathcal{M}_+$  is the set of ground truth correspondence. The subscription in  $\hat{\mathbf{x}}_c^s$  denotes the coefficient selection where  $c$  denotes the selected indices. The triplet loss  $\mathcal{L}_{triplet}$  encourages the descriptiveness of the encoded descriptors  $\hat{\mathbf{x}}^s, \hat{\mathbf{x}}^t$  through the ranking loss  $\mathcal{R}(\hat{\mathbf{x}}_c^s, \hat{\mathbf{x}}_c^t)$  by minimizing the distances of

matched descriptors while maximizing the unmatched ones [27]:

$$\mathcal{R}(\hat{\mathbf{x}}_c^s, \hat{\mathbf{x}}_c^t) = [\mathcal{D}(\hat{\mathbf{x}}_c^s, \hat{\mathbf{x}}_c^t) - m_p]_+ + [m_n - \min_{k \neq c} (\min_{k \neq c} \mathcal{D}(\hat{\mathbf{x}}_c^s, \hat{\mathbf{x}}_k^t), \min_{k \neq c} \mathcal{D}(\hat{\mathbf{x}}_k^s, \hat{\mathbf{x}}_c^t))]_+ \quad (2)$$

where  $m_p$  and  $m_n$  are small constants to prevent the negative loss value. As  $\mathcal{L}_{triplet}$  decreases,  $\mathcal{D}(\hat{\mathbf{x}}_c^s, \hat{\mathbf{x}}_c^t) = \|\hat{\mathbf{x}}_c^s - \hat{\mathbf{x}}_c^t\|_2^2$  for  $c \in \mathcal{M}_+$  will be minimized. Meanwhile, the distance of the wrong matching, *i.e.*,  $\hat{\mathbf{x}}_c^s$  vs.  $\hat{\mathbf{x}}_k^t$  (or  $\hat{\mathbf{x}}_k^s$  vs.  $\hat{\mathbf{x}}_c^t$ ) for  $k \notin \mathcal{M}_+$ , will be further enlarged.

Then, we weigh the distance minimization with confidence  $s_c$  for  $c \in \mathcal{M}_+$ . The confidence  $s_c$  is a scalar product between  $\hat{\mathbf{f}}_c^s$  and  $\hat{\mathbf{f}}_c^t$ , where  $\hat{\mathbf{f}}^s, \hat{\mathbf{f}}^t$  are intermediate outputs from  $\mathcal{F}_\Phi$ , and  $\hat{\mathbf{f}}_c^s, \hat{\mathbf{f}}_c^t$  are column feature vectors:

$$s_c = \hat{\mathbf{f}}_c^{sT} \hat{\mathbf{f}}_c^t \quad (3)$$

The higher confidence  $s_c$  will penalize the feature distance more, resulting in higher descriptiveness, and the lower feature distance can lead to the higher similarity between  $\hat{\mathbf{f}}_c^s$  and  $\hat{\mathbf{f}}_c^t$ , which encourages the matching between keypoints. The proposed loss aims at minimizing the feature distance, which is different from the loss used in the existing works (SuperGlue, SGMNet, and LoFTR) focusing on establishing as many matches as possible with their optimal transport layer, Sinkhorn. Thus, we replace Sinkhorn with feature-distance based matching and filtering (Section 3.5) for the better efficiency.

We implement  $\mathcal{F}_\Phi$  as a Linear Transformer shown in Fig. 4 (Section 3.3) where self- and cross-attention layers collect global information with linear attention [18]. Then, our pairwise neighborhood layers collect the local information from candidate matches. The number of candidate matches is controlled by the global information from the final cross-attention layer in Fig. 4. Thus,  $\hat{\mathbf{f}}^s$  and  $\hat{\mathbf{f}}^t$  in Eq. (3) are the output from this layer. Meanwhile,  $\hat{\mathbf{x}}^s$  and  $\hat{\mathbf{x}}^t$  are the combinations of global and local information from the final layer.

#### 3.2 Efficient Linear Attention

Our Transformer  $\mathcal{F}_\Phi$  contains *multiple encoders*. The function of each encoder is defined by their attention as shown in Fig. 3a. We adopt the architecture of the encoder from [44]. Our Transformer consists of two types of attentional aggregation: (1) *linear attention* [18] and (2) *our pairwise neighborhood attention*.

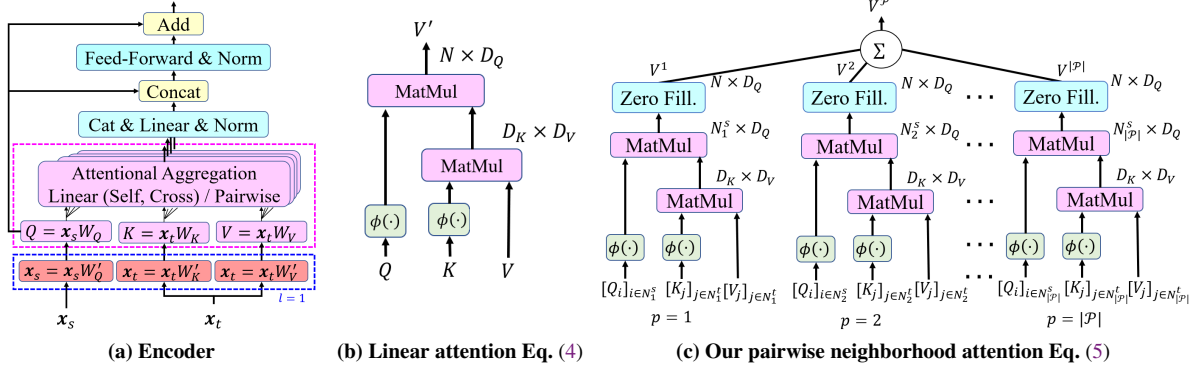


Figure 3: Encoder and attentional aggregation: (a) encoder; (b) linear attention; (c) our pairwise neighborhood attention.

**Linear Attention.** At first, we employ the linear attention similar to [18]. The architecture is provided in Fig. 3b. The inputs of attention are vectors resulting from the linear projection of the source and target descriptors with three matrices  $W_Q \in \mathcal{R}^{D \times D_Q}$ ,  $W_K \in \mathcal{R}^{D \times D_K}$ , and  $W_V \in \mathcal{R}^{D \times D_V}$ . Let  $Q = x_s W_Q$ ,  $K = x_t W_K$ ,  $V = x_t W_V$ . Then, the output from the attention  $V' = \text{LinAtt}(x_s, x_t)$ , is:

$$V' = [V'_i]_{i \in [N]} = \left[ \begin{array}{c} \phi(Q_i)^T \sum_{j \in [M]} \phi(K_j) V_j^T \\ \phi(Q_i)^T \sum_{j \in [M]} \phi(K_j) \end{array} \right]_{i \in [N]} \quad (4)$$

where  $\phi(\cdot) = \text{elu}(\cdot) + 1$ . The subscription  $i$  on a matrix returns a column vector of the  $i$ -th row, e.g.,  $K_j$  is a vector of size  $D_K \times 1$ .

**Pairwise Neighborhood Attention.** To improve Eq. (4), we propose to employ the local information of the neighborhoods area about candidate matches. The architecture is provided in Fig. 3c. Let  $\mathcal{N}_p^s$  and  $\mathcal{N}_p^t$  denote a pair of keypoint neighborhood, where  $\mathcal{N}_p^s$  is from the source, and  $\mathcal{N}_p^t$  from the target. Both center around seed points  $p_1, p_2$  of the matching pair  $p = (p_1, p_2)$ . Thus, our attention incorporates the positional information of the matching neighborhood  $\mathcal{N}_p^s$  and  $\mathcal{N}_p^t$ . The output  $V^p = \text{PairAtt}(x_s, x_t | \mathcal{N}_p^s, \mathcal{N}_p^t)$ , is

$$V^p = [V^p_i]_{i \in \mathcal{N}_p^s} = \left[ \begin{array}{c} \phi(Q_i)^T \sum_{j \in \mathcal{N}_p^t} \phi(K_j) V_j^T \\ \phi(Q_i)^T \sum_{j \in \mathcal{N}_p^t} \phi(K_j) \end{array} \right]_{i \in \mathcal{N}_p^s} \quad (5)$$

Any element outside  $\mathcal{N}_p^s$  is filled with zero value, i.e.,  $V(k)^p = 0$  for  $k \notin \mathcal{N}_p^s$ . If there is more than one pair, the output is a superposition of  $V^p$ , i.e.,  $V^{\mathcal{P}} = \sum_{p \in \mathcal{P}} V^p$  where  $\mathcal{P}$  is the set of matching pairs. The set of neighboring keypoints  $\mathcal{N}_p^s$  (or  $\mathcal{N}_p^t$ ) can be established using a local neighborhood selection (in Section 3.4). An example of the keypoint neighborhood  $\mathcal{N}_p^s$  and  $\mathcal{N}_p^t$  of a matching pair  $p$  is provided in Fig. 2a. The visualization of the attentional aggregation is provided in Fig. 2b, which results in the collection of local information in the pairwise neighborhood. Furthermore, the dominating cost of  $\text{PairAtt}(\cdot)$  is  $O(N_{max} C^2)$  which linearly increases with the largest neighborhood size  $N_{max}$ . The derivation is in Section 3.6.

### 3.3 Network Architecture

Our network architecture is provided in Fig. 4. Each layer consists of an encoder layer (Fig. 3a) with linear or pairwise neighborhood attention, which results in *linear attention layer* and *pairwise neighborhood layer*. We use the linear attention Eq. (4) to perform the self- and cross-attention to collect the global information through

intra- and inter-relationship between descriptors. The self-attention layer updates its message by

$$\hat{x}^s = \text{LinAtt}(x^s, x^s), \quad \hat{x}^t = \text{LinAtt}(x^t, x^t) \quad (6)$$

The cross-attention layer updates messages with information collected from the inter-relationship between two descriptors [36]:

$$\hat{x}^s = \text{LinAtt}(x^s, x^t), \quad \hat{x}^t = \text{LinAtt}(x^t, x^s) \quad (7)$$

Then, we employ our pairwise neighborhood attention Eq. (5) to form the pairwise neighborhood layer that aggregates the local information around candidate matches. We construct a pairwise neighborhood layer using Eq. (5). Given  $(\mathcal{N}_p^s, \mathcal{N}_p^t)$  extracted by the neighborhood selection (Section 3.4), the message update is

$$\begin{aligned} \hat{x}^{sP} &= \text{PairAtt}(x^s, x^t | \mathcal{N}_p^s, \mathcal{N}_p^t), \\ \hat{x}^{tP} &= \text{PairAtt}(x^t, x^s | \mathcal{N}_p^t, \mathcal{N}_p^s) \end{aligned} \quad (8)$$

where any element outside  $\mathcal{N}_p^s$  is filled with zero value, i.e.,  $\hat{x}^s(k)^p = 0$  for  $k \notin \mathcal{N}_p^s$  and  $\hat{x}^t(k)^p = 0$  for  $k \notin \mathcal{N}_p^t$ . Finally,  $\hat{x}^s = \sum_{p \in \mathcal{P}} \hat{x}^{sP}$  and  $\hat{x}^t = \sum_{p \in \mathcal{P}} \hat{x}^{tP}$ . Then, we perform  $L_1$  loop updates between self- and cross-attention layers, and  $L_2$  loop updates over the pairwise neighborhood layer. Unlike [5, 36, 44], we did not employ any positional encoder. In addition, our first layer ( $l = 1$ ) has additional linear weights  $W'_Q, W'_K$ , and  $W'_V$  to reduce the dimension of input descriptors into the lower dimensions  $D_Q, D_K$ , and  $D_V$ , leading to the lower computational cost in the multi-head attention of the subsequent layers [49]. Here, we set  $D_Q, D_K, D_V = C'$ .

### 3.4 Local Neighborhood Selection

We track the local information from candidate matches for pairwise neighborhood layers as follows. We employ  $f^s$  and  $f^t$  from the final cross-attention layer to extract the matching pairs. Then, we construct the set of hypothesis matching seeds  $\mathcal{P}$ , which ensures that the seeds well spread across images. Finally, we extract the set of neighborhoods compatible with the matching seeds to construct the keypoint neighborhood, i.e.,  $\mathcal{N}_p^s$  and  $\mathcal{N}_p^t$ , for  $p \in \mathcal{P}$ , for Eq. (5).

**Hypothesis Matching Seeds Selection.** We start from establishing the set of seed points with high matching confidence and well spread around the image. Let  $\mathcal{M}$  denotes a set containing the matching pair extracted by the distance ratio algorithm  $\text{Dist}(\cdot, |\theta)$  [26] where  $\theta$  is an appropriate threshold. Let  $\text{distratio}(i, j)$  denotes the distance ratio

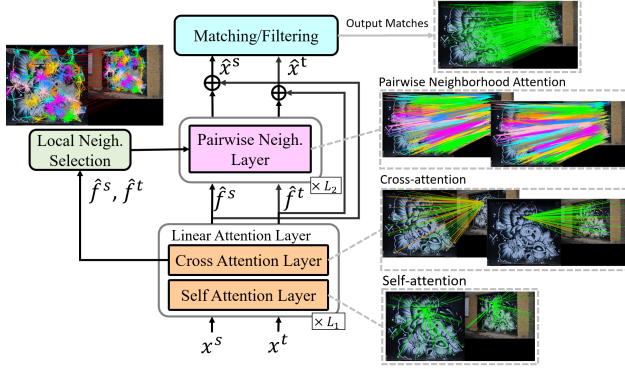


Figure 4: Network Architecture

value corresponding to the match  $(i, j)$ . Then, the set of matching seeds is defined as follows:

$$\mathcal{P} := \{(i, j) \mid \text{distratio}(i, j) > \text{distratio}(i, k), \\ \text{for } k \in \text{Nei}(j|R), \forall (i, j) \in \mathcal{M}\} \quad (9)$$

where  $\text{Nei}(\cdot|R)$  denotes the index set of neighboring keypoints within radius  $R$ . We follow [4] to employ the seed separation condition where the match index  $(i, j)$  is selected to the set of matching seeds  $\mathcal{P}$ , if it has the highest distance ratio among its local neighbors. This is to ensure that the matching seeds are well spread.

**Local Neighborhood Set Selection.** To include candidate matches that are geometrically consistent with the matching seed  $p \in \mathcal{P}$ , we collect the points that locate in a similar neighborhood, following [4, 37]. Let  $(k_p^s, k_p^t)$  denote the location of the matched keypoints from source to target corresponding to the matching seed  $p \in \mathcal{P}$ . The local neighborhood set  $\mathcal{N}_p$  is defined as:

$$\mathcal{N}_p := \{(p_1, p_2) \mid \|k_{p_1}^s - k_p^s\| \leq \lambda R_s \ \& \ \|k_{p_2}^t - k_p^t\| \leq \lambda R_t, \\ \forall (p_1, p_2) \in \mathcal{M}\} \quad (10)$$

where  $R_s$  and  $R_t$  are the radii to control the coverage of neighboring points around the matching seed  $p$  in  $I_s$  and  $I_t$ , respectively.  $\lambda$  is a hyperparameter that regulates the overlapping between neighborhoods. Then, the pair of keypoint neighborhood  $(\mathcal{N}_p^s, \mathcal{N}_p^t)$  is defined as:

$$\mathcal{N}_p^s := \{i \mid i : (i, j) \in \mathcal{N}_p\}, \quad \mathcal{N}_p^t := \{j \mid j : (i, j) \in \mathcal{N}_p\} \quad (11)$$

The pair of keypoint neighborhood  $\mathcal{N}_p^s, \mathcal{N}_p^t$  will be used to define the aggregation in Eq. (5) to emphasize the area of candidate matches.

### 3.5 Feature distance-based matching and filtering

Given the descriptors  $\hat{x}^s, \hat{x}^t$  from our Transformer, one can obtain the set of match pairs  $\mathcal{M}_c$  by distance ratio thresholding such as [26]. However, the fixed thresholding value tends to restrict the candidate matches overly. Thus, we employ the similar procedure to Section 3.4 to include the candidate matches compatible with  $\mathcal{M}_c$ :

- (1) Extract hypothesis matching seeds  $\mathcal{P}_c$  with Eq. (9) where  $\hat{x}_s, \hat{x}_t$  are used to construct the set of matching pairs  $\mathcal{M}_c$ .
- (2) Extract the set of candidate matches, i.e.,  $\{\mathcal{N}_c \mid c \in \mathcal{P}_c\}$  where  $\mathcal{N}_c$  is extracted with Eq. (10).

**Filtering.** We employ the filtering process of AdaLAM [4] (without refitting) to improve the performance by verifying the local affine

Table 2: Time Complexity of Linear Attention

Step	Operation	Input	Output	Complexity
1. Numerator	$\sum_{j \in [M]} \phi(K_j) V_j^T$	two $[C' \times 1]$	$K_o = [C' \times C']$	$O(MC'^2)$
	$\phi(Q_i)^T K_o$	$[C' \times 1], [C' \times C']$	$Q_k^T = [1 \times C']$	$O(C'^2)$
2. Denominator	$\sum_{j \in [M]} \phi(K_j)$	$[C' \times 1]$	$K_m = [C' \times 1]$	$O(M)$
	$\phi(Q_i)^T K_m$	two $[C' \times 1]$	$Den_i = [1 \times 1]$	$O(C')$
3. Final	$Q_k^T / Den$	$[1 \times C'], [1 \times 1]$	$V_i'^T = [1 \times C']$	$O(C')$
	$[V_i']_{i \in N}$	$[C' \times 1]$	$V' = [N \times C']$	$O(NC')$

Table 3: Time Complexity of Pairwise Neighborhood Attention

Step	Operation	Input	Output	Complexity
1. Numerator	$\sum_{j \in \mathcal{N}_p^t} \phi(K_j) V_j^T$	two $[C' \times 1]$	$K_o = [C' \times C']$	$O( \mathcal{N}_p^t C'^2)$
	$\phi(Q_i)^T K_o$	$[C' \times 1], [C' \times C']$	$Q_k^T = [1 \times C']$	$O(C'^2)$
2. Denominator	$\sum_{j \in \mathcal{N}_p^t} \phi(K_j)$	$[C' \times 1]$	$K_m = [C' \times 1]$	$O( \mathcal{N}_p^t )$
	$\phi(Q_i)^T K_m$	two $[C' \times 1]$	$Den_i = [1 \times 1]$	$O(C')$
3. Final	$Q_k^T / Den$	$[1 \times C'], [1 \times 1]$	$V_i'^T = [1 \times C']$	$O(C')$
	$[V_i']_{i \in \mathcal{N}_p^s}$	$[C' \times 1]$	$V' = [ \mathcal{N}_p^s  \times C']$	$O( \mathcal{N}_p^s C')$

consistency in each  $\mathcal{N}_c$  with highly parallel RANSACs [4, 14]. The filtering scales well with the high number of keypoints ( $> 10,000$ ).

The resulting matches  $\{\mathcal{N}_c \mid c \in \mathcal{P}_c\}$  could contain many wrong matches; however, using our network with such procedure (denoted as distance matching or **DM**) provides comparable performance to AdaLAM [4] in most cases (see Table 4). The filtering process in AdaLAM (**Filter**) improves the performance further, yet the performance gain is more obvious with our pairwise neighborhood layer. It can be shown that the runtime cost of the feature distance-based matching and filtering is much lower than Sinkhorn that is used by SuperGlue and SGMNet from Table 6, and using linear transformer with Sinkhorn does not lead to higher matches (see Section D).

### 3.6 Time Complexity

This section provides the time complexity of the two attentional aggregation used in our work: *linear attention* Eq. (4) and our *pairwise neighborhood attention* Eq. (5). Our derivation is based on the size of  $Q, \phi(Q) \in \mathcal{R}^{N \times C'}$  and  $K, V, \phi(K) \in \mathcal{R}^{M \times C'}$ .

**Linear Attention.** The complexity of Eq. (4) is derived as in Table 2. The analysis starts from the computations in numerator *Step.1*, denominator *Step.2*, and final division *Step.3*. The total complexity is  $O(MC'^2 + C'^2 + M + C' + C' + NC') \approx O(MC'^2)$ .

**Pairwise neighborhood attention.** The time complexity of Eq. (5) is derived similarly in Table 3. The only difference is the range of summation operations. The total complexity is  $O(|\mathcal{N}_p^t|C'^2 + C'^2 + |\mathcal{N}_p^t| + C' + C' + |\mathcal{N}_p^s|C')$ . Let  $N_{max}$  denote the size of the largest neighborhood among  $\mathcal{N}_p^t$  for  $p \in \mathcal{P}$ , i.e.,  $N_{max} = \max_{p \in \mathcal{P}} |\mathcal{N}_p^t|$ . Thus, the dominating complexity is  $\approx O(N_{max}C'^2)$ .

**Total.** Combining the two, we obtain  $O(MC'^2 + N_{max}C'^2) \approx O(MC'^2)$  for  $N_{max} \ll M$ . Table 1 provides the comparison with SOTAs. Among these methods, our time complexity linear to  $M$  (or  $N$ ). In practice, we set  $\mathcal{N}_p^s$  (or  $\mathcal{N}_p^t$ ) to the same size for parallel computation.

## 4 Experimental Results

We provide the ablation study and the scalability of our work against SOTAs. Then, our method is evaluated on several practical scenarios,



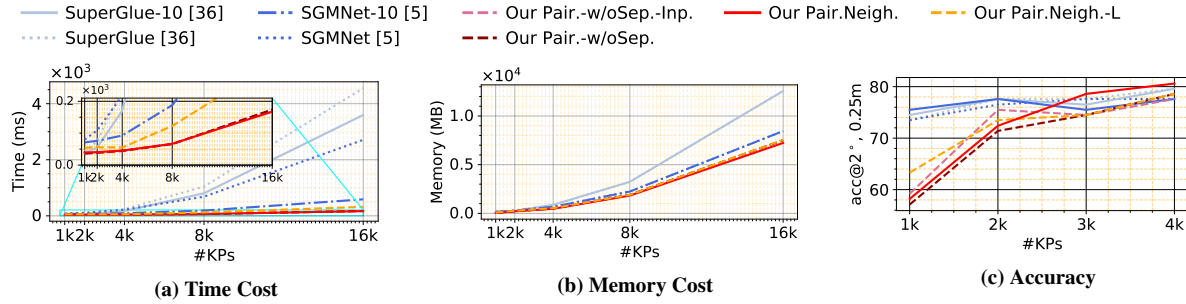


**Figure 5: Overall scalability. Our proposed method versus SOTA matching, Superglue and SGMNet with the official settings and Superglue and SGMNet with the faster runtime (denoted as -10 for Sinkhorn iter. = 10).**

*i.e.*, image matching, 3D reconstruction, and visual localization. The model implementation and training are provided in *suppl. A*.

**Comparative methods.** Our work is compared with **1) Sparse matching:** SuperGlue [36] and SGMNet [5]. **2) Dense matching:** LoFTR [44], Patch2Pix [55], NCNet [33]. **3) Local features:** SuperPoint [11], R2D2 [32], D2-Net [12], and ASLFeat [27], where the standard matching, *e.g.*, *MNN*-matching or Lowe’s Thresholding, is used for matching local features. **4) Keypoint filtering:** AdaLAM [4] and OANet [54]. We report either results from **the original papers** or derived from **the official implementations** with default settings unless otherwise specified. In each table, we highlight the *top two* or *top three* and *underline* the best result.

In this paper, we apply our method to match the local features of **SuperPoint** [11] where keypoints are limited to 2k for image matching, 10k for 3D Reconstruction, and 4k for visual localization.

## 4.1 Ablation Study

This study uses localization accuracy on Aachen Day-Night [38, 40].

**Ablation Study on the Proposed Networks.** We provide the ablation study on the impact of each component in our network Fig. 4, *i.e.*, linear attention layer, pairwise neighborhood layer, feature distance-based matching and filtering, and encoded feature dimensions.

From Table 4, our *Pair.Neigh.* with both linear attention layer (**LA**) and pairwise neighborhood layer (**PN**) offers the higher accuracy than *Linear.* that uses only linear attention layer, in most cases, from 1k to 4k keypoints. Using filtering (**Filt.**) further improves the accuracy, especially for *Pair.Neigh.*. Next, we compare the model size defined by **#dim**. The large-size model (L) offers the higher robustness, yet our small model (S) offers the better trade-off with the computational cost. Since the goal is to achieve the high efficiency, our small model is used in subsequent comparisons against SOTAs.

**Configuration of Local Neighbor Selection.** We consider three configurations: • *Pair.-w/oSep-Inp.* omits the seed separation in Eq. (9) & uses  $x^s, x^t$ , instead of  $f^{ss}, f^{tt}$ , in Fig. 4 for *Local Neigh. Selection*. • *Pair.-w/oSep.* omits the seed separation in Eq. (9) and uses  $f^{ss}, f^{tt}$  as input for *Local Neigh. Selection*. • *Pair.Neigh.* follows all the steps, similar to *No.5* in Table 4.

Table 5 shows that our *Pair.Neigh.* and *Pair.-w/oSep.* offer the highest accuracy when the number of keypoints is high (>2k). Meanwhile, *Pair.-w/oSep-Inp.* offers higher robustness when the number of keypoints is low. Notice that all of them offer higher accuracy than using only *Linear Attention (No.4)*. We report the results of

**Table 4: Impact of each component in our network (Fig. 4).**

No.	Methods	Configurations					Accuracy @ 0.25m, 2°			
		LA	PN	DM	Filt.	#dim size	1k	2k	3k	4k
1	AdaLAM [4]	-	-	✓	✓	256 -	41.8	71.4	<u>79.6</u>	76.5
2	Our <i>Linear.</i> (No Filt.)	$L_1=10$	✗	✓	✗	64 S	61.2	72.4	73.5	76.5
3	Our <i>Pair.Neigh.</i> (No Filt.)	$L_1=8$	$L_2=2$	✓	✗	64 S	<u>66.3</u>	<u>74.5</u>	73.5	76.5
4	Our <i>Linear.</i>	$L_1=10$	✗	✓	✓	64 S	48.0	<u>73.5</u>	76.5	77.6
5	Our <i>Pair.Neigh.</i>	$L_1=8$	$L_2=2$	✓	✓	64 S	58.2	72.4	<u>78.6</u>	<u>80.6</u>
6	Our <i>Pair.Neigh.-L</i>	$L_1=8$	$L_2=2$	✓	✓	256 L	<u>63.3</u>	<u>73.5</u>	74.5	<u>78.6</u>

**LA:** Linear Attention layer, **PN:** Pairwise Neighborhood Attention layer, **DM:** Distance Matching, **#dim:** Feature dimension  $C'$ , **size:** Network size large(L) / small(S).

**Table 5: Configurations of local neighborhood selection.**

Methods	Config. of Local Neigh. Selection		Accuracy @ 0.25m, 2°			
	Inputs	Seed separation Eq. (9)	1k	2k	3k	4k
<i>Pair.-w/oSep-Inp.</i>	$x^s, x^t$	✗	<u>59.2</u>	<u>75.5</u>	<u>74.5</u>	77.6
<i>Pair.-w/oSep.</i>	$f^{ss}, f^{tt}$	✗	57.1	71.4	<u>74.5</u>	<u>78.6</u>
<i>Pair.Neigh.</i>	$f^{ss}, f^{tt}$	✓	<u>58.2</u>	<u>72.4</u>	<u>78.6</u>	<u>80.6</u>

three configurations in the next SOTAs comparison. The detailed results across all the error tolerances, *i.e.*, (0.25m, 2°), (0.5m, 5°), and (5m, 10°), and visualization are provided in *suppl. E*.

## 4.2 Overall Scalability

We confirm the overall performance of our work on time and memory cost when running inference in Fig. 5. All the reported results are based on the official settings and run in real-time on a Titan RTX. In the official SuperGlue and SGMNet, the Sinkhorn iteration is set to 100. We also compare against SuperGlue-10 and SGMNet-10 where Sinkhorn iteration set to 10. We also report our large-size model (Our *Pair.Neigh.-L*), with the same settings as *No.6* in Table 4.

**Time Cost.** From Fig. 5a, our time cost is remarkably lower than SuperGlue and SGMNet and is *linear* with the number of keypoints (**#kpt**). Specifically, at 16k keypoints, our method is about 28 and 9 times faster than the official SuperGlue and SGMNet and is about 21 and 3 times faster than SuperGlue-10 and SGMNet-10. Our large model has higher runtime yet is much faster than the SOTAs.

**Memory Cost.** In Fig. 5b, we measure the memory cost using the peak of memory consumption similar to [5]. Our method consumes lower memory than SuperGlue and SGMNet even when the number

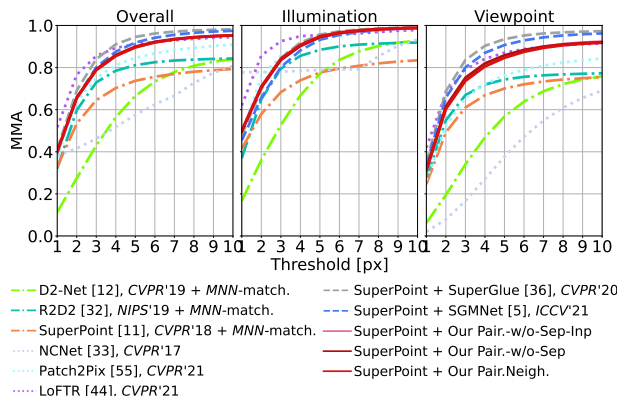


**Figure 6: Image matching. Our method versus SOTAs— local features, dense matching, and sparse matching—on HPatches dataset [3]. We report *MMA* across error thresholds (1-10 *px*), the number of matches (*#Matches*), averaged ratios of the inliers (*Inl.Ratio*), the number of learnable parameters (*#Param.*), and *Total Time*<sup>‡</sup>.**

Methods	Pub.	#Matches	Inl.Ratio	#Param.	Total Time(ms) <sup>‡</sup>
D2-Net [12] + <i>MNN</i> -matching	CVPR'19	$2.50 \times 10^3$	0.42	$7.64 \times 10^6$	487.06
R2D2 [32] + <i>MNN</i> -matching	NIPS'19	$2.05 \times 10^3$	0.74	$1.04 \times 10^6$	1755.16
SuperPoint [11] + <i>MNN</i> -matching	CVPR'18	$1.08 \times 10^3$	0.65	$1.30 \times 10^6$	<b>34.30</b>
NCNet [33]	CVPR'17	$1.48 \times 10^3$	0.46	$21.3 \times 10^6$	297.18
Patch2Pix [55]	CVPR'21	$1.26 \times 10^3$	0.76	$31.6 \times 10^6$	453.07
LoFTR [44]	CVPR'21	$4.71 \times 10^3$	<b>0.87</b>	$11.6 \times 10^6$	212.98
SuperPoint + SuperGlue [36]	CVPR'20	$8.32 \times 10^2$	<b>0.84</b>	$12.0 \times 10^6$	115.14
SuperPoint + SGMNet [5]	ICCV'21	$8.66 \times 10^2$	0.80	$31.1 \times 10^6$	116.11
SuperPoint + Our <i>Pair.-w/oSep-Inp.</i>	—	$7.15 \times 10^2$	0.80	<b><math>0.841 \times 10^6</math></b>	<b>68.49</b>
SuperPoint + Our <i>Pair.-w/oSep.</i>	—	$6.97 \times 10^2$	<b>0.81</b>	<b><math>0.841 \times 10^6</math></b>	<b>68.58</b>
SuperPoint + Our <i>Pair.Neigh.</i>	—	$7.11 \times 10^2$	0.80	<b><math>0.841 \times 10^6</math></b>	73.52

<sup>‡</sup> Total Time = Feature Extraction Time + Sparse/Dense Matching Time.

**Table 6: Individual runtime: (a) Transformer & (b) Matching.**

Methods	(a) Transformer (ms)				(b) Matching (ms)						
	#Param	<i>Cplx.</i>	2k	4k	8k	16k	Type	2k	4k	8k	16k
SuperGlue [36]	12M	$N^2C$	53	163	752	3392	Sink.	22	78	292	1162
SGMNet [5]	30M	$NKC + K^2C$	70	77	122	341	Sink.	39	140	562	2370
Our <i>Pair.Neigh.</i>	0.8M	$\approx NC^2$	<b>34</b>	<b>35</b>	<b>44</b>	<b>100</b>	DF	<b>7</b>	<b>10</b>	<b>22</b>	<b>67</b>
Our <i>Pair.Neigh.-L</i>	12M	$\approx NC^2$	<b>51</b>	<b>45</b>	<b>96</b>	<b>235</b>	DF	<b>5</b>	<b>10</b>	<b>26</b>	<b>84</b>

Sink: Sinkhorn, DF: Distance Matching & Filtering.  
Our *Pair.Neigh.-L*: the setting is similar to *No.6* in Table 4.

of keypoints is as low as 1k. When the number of keypoints  $\geq 4k$ , our GPU memory cost is 50% and 20% lower than SuperGlue and SGMNet, respectively. Our large-size model consumes slightly higher memory, which resonates with the advantage of linear attention [18].

**Accuracy vs. Keypoints.** Fig. 5c demonstrates the impact on visual localization accuracy (0.25m,  $2^\circ$ ) as the number of keypoints increases. For our work, the impact on visual localization accuracy is more obvious as the keypoints increase. Meanwhile, SuperGlue and SGMNet only slightly improve with the number of keypoints. Our work outperforms both when the number of keypoints is  $\geq 3k$ .

**Runtime of Individual Parts.** Table 6 provides the time cost of the individual parts: (a) Transformer and (b) matching. Our runtime increases with a much lower rate for both parts. Our large-size model (L) behaves similarly. This confirms the superior efficiency of our linear attention against the regular softmax attention of the SOTAs, as well as the faster speed of our distance-based matching and filtering over Sinkhorn used in SuperGlue and SGMNet.

### 4.3 Image Matching

This section we compare the image matching performance between our method against the SOTA *local features*, *dense matching*, and *sparse matching* on HPatches [3] following the protocol of [12]. The additional visual results are provided in *suppl. F.1*.

**Local Features.** In Fig. 6, our *MMA* curves surpass all the SOTA local features D2-Net, R2D2, and SuperPoint with *MNN*-matching

(baseline). Notice that our *Total Time* also includes the feature extraction runtime of SuperPoint.

**Dense Matching.** In overall and viewpoint changes, our methods achieve similar *MMA* curves to LoFTR. LoFTR also offers the highest *Inl.Ratio* and *#Matches*. However, *Total Time* of LoFTR is about three times that of our method. Patch2Pix also provides high *MMA*, but the *Total Time* is about six times of ours.

**Sparse Matching.** Our methods offer slightly lower *MMA* and *#Matches*, and a similar *Inl.Ratio* compared to SuperGlue and SGMNet. However, we can realize this performance with 1/10 *#Param.* and half *Total Time*. Our study on scalability (Section 4.2) reveals the efficiency improvement by our methods.

### 4.4 3D Reconstruction

**Evaluation.** 3D reconstruction is a keypoint-consuming application; thus, we report the matching runtime (*Match. Time*) to indicate the efficiency alongside other indicators. We follow the ETH evaluation [42] where sparse and dense reconstruction are performed by the SfM and MVS from COLMAP [41]. The dense points are from the dense reconstruction. Detailed settings and visual results are provided in *suppl. C.1* and *suppl. F.2*.

Our method is compared against the official SuperGlue and SGMNet and SuperGlue-10 and SGMNet-10 in Table 7. Because the official implementations take too much runtime on the medium-size datasets, we compare our method against SuperGlue-10 and SGMNet-10 in Table 8. We also report AdaLAM and *MNN*+Lowe's Threshold [26].

**Results on Small-size ETH.** From Table 7, our methods provide the longest *Track. Len.*, with lower *Reproj. Error*, and comparable *Dense Points* to SuperGlue, SuperGlue-10, SGMNet, and SGMNet-10. Our *Match. Time* is about **10 times** and **3 times faster** than SuperGlue-10 and SGMNet-10, respectively. Compared with SuperGlue and SGMNet with the official settings, the efficiency gap of our work becomes larger. Our *Match. Time* is at least **20 times** and about **8 times faster** than SuperGlue and SGMNet, respectively.

**Results on Medium-size ETH.** From Table 8, our method provides the longest *Track. Len.* and low *Reproj. Error* in most cases. Our method offers moderate *Dense Points* with lower runtime than

**Table 7: Small-size ETH. Our methods versus the official SuperGlue and SGMNet, Superglue-10 and SGMet-10.**

Datasets	Methods	Track. Len.	Reproj. Error	Sparse Points	Dense Points	Match. Time(sec)
Herzjesu 8 images	SuperGlue [36] <sup>†</sup>	4.45	0.921	<b>8.5k</b>	1.14M	$4.71 \times 10^2$
	SuperGlue-10 [36]	4.44	0.921	<b>8.5k</b>	<b>1.15M</b>	$2.68 \times 10^2$
	SGMNet [5] <sup>§</sup>	4.16	0.960	<b>9.6k</b>	1.14M	$1.43 \times 10^2$
	SGMNet-10 [5]	4.14	0.955	<b>9.8k</b>	1.14M	$0.66 \times 10^2$
	Our <i>Pair.-w/oSep.-Inp.</i>	<b>4.54</b>	<b>0.881</b>	7.3k	<b>1.14M</b>	<b><math>0.24 \times 10^2</math></b>
	Our <i>Pair.-w/oSep.</i>	<b>4.54</b>	<b>0.872</b>	7.2k	<b>1.15M</b>	<b><math>0.24 \times 10^2</math></b>
Our <i>Pair.Neigh.</i>	<b>4.53</b>	<b>0.873</b>	7.3k	<b>1.14M</b>	<b><math>0.23 \times 10^2</math></b>	
Fountain 11 images	SuperGlue [36] <sup>†</sup>	5.14	0.961	<b>11.4k</b>	<b>1.84M</b>	$7.90 \times 10^2$
	SuperGlue-10 [36]	5.14	0.960	<b>11.4k</b>	1.83M	$4.42 \times 10^2$
	SGMNet [5] <sup>§</sup>	4.93	0.959	<b>11.9k</b>	<b>1.84M</b>	$2.38 \times 10^2$
	SGMNet-10 [5]	4.92	0.966	<b>11.9k</b>	<b>1.84M</b>	$1.12 \times 10^2$
	Our <i>Pair.-w/oSep.-Inp.</i>	<b>5.17</b>	<b>0.909</b>	10.0k	1.83M	<b><math>0.41 \times 10^2</math></b>
	Our <i>Pair.-w/oSep.</i>	<b>5.16</b>	<b>0.905</b>	10.0k	1.83M	<b><math>0.42 \times 10^2</math></b>
Our <i>Pair.Neigh.</i>	<b>5.14</b>	<b>0.903</b>	10.0k	1.83M	<b><math>0.41 \times 10^2</math></b>	
South-Building 128 images	SuperGlue [36] <sup>†</sup>	7.90	0.947	114.4k	<b>12.53M</b>	$402.23 \times 10^2$
	SuperGlue-10 [36]	7.88	0.949	<b>114.8k</b>	<b>12.51M</b>	$228.43 \times 10^2$
	SGMNet [5] <sup>§</sup>	6.95	0.979	<b>132.2k</b>	12.39M	$108.67 \times 10^2$
	SGMNet-10 [5]	6.97	0.981	<b>131.2k</b>	12.33M	$48.79 \times 10^2$
	Our <i>Pair.-w/oSep.-Inp.</i>	<b>8.31</b>	<b>0.837</b>	94.8k	12.40M	<b><math>14.83 \times 10^2</math></b>
	Our <i>Pair.-w/oSep.</i>	<b>8.31</b>	<b>0.832</b>	94.2k	12.42M	<b><math>13.86 \times 10^2</math></b>
Our <i>Pair.Neigh.</i>	<b>8.27</b>	<b>0.836</b>	95.1k	<b>12.45M</b>	<b><math>13.29 \times 10^2</math></b>	

<sup>†</sup> SuperGlue with its official setting (Sinkhorn iter. = 100).

<sup>§</sup> SGMNet with its official setting (Sinkhorn iter. = 100, num. seeds = 128).

SuperGlue-10 and SGMNet-10. The baseline [26] provides the lowest reprojection error. However, our methods provide longer tracking length and higher *#Reg. Img.* to AdaLAM and the baseline in most cases. Our *Dense Points* is also higher than these two approaches and is comparable with SuperGlue-10 and SGMNet-10, suggesting the similar visual quality of the 3D reconstruction. Our *Match. Time* is about **3 times** and **twice faster** than SuperGlue-10 and SGMNet-10, due to the lower detected keypoints by SuperPoint.

## 4.5 Visual Localization

**Evaluation.** We employ the Aachen Day-Night [38, 40] to demonstrate the effect on visual localization. We follow the evaluation protocols of *Visual Localization Benchmark*<sup>†</sup> and report the percent of successfully localized images. The full results of our works with different configurations are provided in Table 16.

**Results.** From Table 9, our method gives the competitive accuracy at (0.25m, 2°): our *Pair.Neigh.*<sup>‡</sup> gives the highest accuracy among the methods that employ SuperPoint as input features, *i.e.*, the sparse matching (SuperGlue, SGMNet) and the keypoint filtering (OANet, AdaLAM). Meanwhile, our *Pair.-w/oSep.* offers higher accuracy than SGMNet but lower than SuperGlue. Our performance drops as the error threshold becomes less restrictive and is on par with AdaLAM. This suggests that our method is more accurate but less robust, as our works tend to provide less matches than SuperGlue and SGMNet. Nevertheless, our methods can achieve this with a much lower *#Param.* and *#dim.* Compared to the SOTA local features, we use only 4k keypoints but give the closest performance to ASLFeat.

<sup>†</sup> More details about settings are in *suppl. C.2*.

<sup>‡</sup> Official result is provided on [visuallocalization.net](http://visuallocalization.net) as EffLinAtt+Superpoint-4K

**Table 8: Medium-size ETH. Our method versus MNN+Lowe’s Thresholding, AdaLAM, Superglue-10, and SGMNet-10.**

Datasets	Methods	Track. Len.	Reproj. Error	#Reg. Img.	Dense Points	Match. Time (H:M:S)
Madrid Metropolis 1344 images	MNN+Lowe’s.(baseline) [26]	7.28	<b>1.066</b>	513	2.95M	<b>00:04:51</b>
	AdaLAM [4]	<b>8.29</b>	<b>1.113</b>	519	<b>3.04M</b>	<b>00:10:44</b>
	SuperGlue-10 [36]	7.59	1.240	<b>732</b>	<b>3.39M</b>	05:15:30
	SGMNet-10 [5]	6.99	1.211	<b>759</b>	<b>3.44M</b>	05:27:46
	Our <i>Pair.-w/oSep.-Inp.</i>	8.19	<b>1.106</b>	<b>563</b>	2.54M	<b>01:16:21</b>
	Our <i>Pair.-w/oSep.</i>	<b>8.67</b>	1.114	508	2.88M	02:40:49
Our <i>Pair.Neigh.</i>	<b>8.51</b>	1.118	523	3.02M	01:22:36	
Gendarmenmarkt 1463 images	MNN+Lowe’s.(baseline) [26]	6.57	<b>1.069</b>	1034	<b>7.12M</b>	<b>00:05:23</b>
	AdaLAM [4]	<b>8.05</b>	1.135	<b>1041</b>	6.77M	<b>00:20:43</b>
	SuperGlue-10 [36]	<b>8.36</b>	1.222	<b>1060</b>	<b>7.24M</b>	07:08:39
	SGMNet-10 [5]	7.53	1.203	<b>1124</b>	6.64M	05:12:59
	Our <i>Pair.-w/oSep.-Inp.</i>	7.89	1.117	1039	7.00M	02:29:20
	Our <i>Pair.-w/oSep.</i>	7.91	<b>1.103</b>	1039	<b>7.06M</b>	02:56:32
Our <i>Pair.Neigh.</i>	<b>7.92</b>	<b>1.116</b>	1030	6.96M	<b>02:02:18</b>	
Tower of London 1576 images	MNN+Lowe’s.(baseline) [26]	7.44	<b>1.014</b>	733	5.09M	<b>00:05:49</b>
	AdaLAM [4]	8.46	1.044	777	5.47M	<b>00:13:28</b>
	SuperGlue-10 [36]	7.27	1.145	<b>941</b>	<b>5.97M</b>	06:22:13
	SGMNet-10 [5]	6.78	1.145	<b>879</b>	<b>5.66M</b>	05:02:00
	Our <i>Pair.-w/oSep.-Inp.</i>	<b>8.51</b>	1.041	766	<b>5.53M</b>	02:17:24
	Our <i>Pair.-w/oSep.</i>	<b>8.63</b>	<b>1.040</b>	776	5.41M	03:19:36
Our <i>Pair.Neigh.</i>	<b>8.49</b>	<b>1.038</b>	<b>779</b>	5.43M	<b>01:46:00</b>	

**Table 9: Visual localization on the Aachen Day-Night against SOTA local features, keypoint filtering, and sparse matching.**

Methods	#kpts	#dim	#Param.	Pub.	Cplx.	0.25m, 2°	0.5m, 5°	5m, 10°
D2-Net [12]	19K	512	15M	CVPR’19	-	74.5	86.7	<b>100.0</b>
ASLFeat [27] v.2	10K	128	<b>0.4M</b>	CVPR’20	-	<b>81.6</b>	87.8	<b>100.0</b>
R2D2 [32] N = 8	40K	128	1.0M	NIPS’19	-	76.5	<b>90.8</b>	<b>100.0</b>
SPTD2 [52]	10K	128	-	IJCV’21	-	78.8	<b>89.3</b>	<b>99.0</b>
SuperPoint [11] + SOTA Filtering/Matching								
↳ Baseline MNN	<b>4K</b>	256	-	CVPR’18	-	71.4	78.6	87.8
↳ + OANet [54]	<b>4K</b>	256	4.8M	ICCV’19	-	77.6	<b>90.8</b>	<b>100.0</b>
↳ + AdaLAM [4]	<b>4K</b>	256	-	ECCV’20	-	76.5	86.7	95.9
↳ + SuperGlue [36]	<b>4K</b>	256	12M	CVPR’20	N <sup>2</sup> C	79.6	<b>90.8</b>	<b>100.0</b>
↳ + SGMNet [5]	<b>4K</b>	256	31M	ICCV’21	NKC+K <sup>2</sup> C	77.6	88.8	<b>99.0</b>
↳ + Our <i>Pair.-w/oSep.</i>	<b>4K</b>	<b>64</b>	<b>0.8M</b>	-	≈ NC <sup>2</sup>	78.6	86.7	95.9
↳ + Our <i>Pair.Neigh.</i>	<b>4K</b>	<b>64</b>	<b>0.8M</b>	-	≈ NC <sup>2</sup>	<b>80.6</b>	86.7	95.9
↳ + Our <i>Pair.Neigh.-L</i>	<b>4K</b>	256	12M	-	≈ NC <sup>2</sup>	78.6	87.8	96.9

## 5 Summary

To improve the efficiency of existing SOTA Transformers in sparse matching applications, we propose efficient attention that offers linear time complexity and high accuracy by aggregating the local and global formation. To keep the high efficiency, we proposed to train the Transformer with the joint learning of the sparse matching and description optimized based on the feature distance. This enables the use of feature distance-based matching and filtering that is simpler and faster than Sinkhorn, which results in high accuracy and extremely low runtime. Extensive experiments indicate a significant improvement in efficiency against the bigger SOTAs.



## References

- [1] Hassan Abu Alhaija, Anita Sellent, Daniel Kondermann, and Carsten Rother. 2015. GraphFlow – 6D Large Displacement Scene Flow via Graph Matching. In *Pattern Recognition*, Juergen Gall, Peter Gehler, and Bastian Leibe (Eds.). Springer International Publishing, Cham, 285–296.
- [2] R. Arandjelović, P. Gronat, A. Torii, T. Pajdla, and J. Sivic. 2018. NetVLAD: CNN architecture for weakly supervised place recognition. *IEEE Transactions on Pattern Analysis and Machine Intelligence* 40, 6 (2018), 1437–1451.
- [3] V. Balntas, K. Lenc, A. Vedaldi, and K. Mikolajczyk. 2017. HPatches: A benchmark and evaluation of handcrafted and learned local descriptors. In *Proceedings of IEEE Conference on Computer Vision and Pattern Recognition (CVPR)*.
- [4] Luca Cavalli, Viktor Larsson, Martin Ralf Oswald, Torsten Sattler, and Marc Pollefeys. 2020. Handcrafted Outlier Detection Revisited. In *Proceedings of the European Conference on Computer Vision*.
- [5] Hongkai Chen, Zixin Luo, Jiahui Zhang, Lei Zhou, Xuyang Bai, Zeyu Hu, Chiew-Lan Tai, and Long Quan. 2021. Learning to Match Features with Seeded Graph Matching Network. In *International Conference on Computer Vision (ICCV)*.
- [6] Hwann-Tzong Chen, Horng-Horng Lin, and Tyng-Luh Liu. 2001. Multi-object tracking using dynamical graph matching. In *IEEE Computer Society Conference on Computer Vision and Pattern Recognition (CVPR)*, Vol. 2. II–II. <https://doi.org/10.1109/CVPR.2001.990962>
- [7] Rewon Child, Scott Gray, Alec Radford, and Ilya Sutskever. 2019. Generating Long Sequences with Sparse Transformers. URL <https://openai.com/blog/sparse-transformers> (2019).
- [8] Krzysztof Marcin Choromanski, Valerii Likhoshesterov, David Dohan, Xingyou Song, Andreea Gane, Tamas Sarlos, Peter Hawkins, Jared Quincy Davis, Afroz Mohiuddin, Lukasz Kaiser, David Benjamin Belanger, Lucy J Colwell, and Adrian Weller. 2021. Rethinking Attention with Performers. In *International Conference on Learning Representations*. <https://openreview.net/forum?id=Ua6zuk0WRH>
- [9] Marco Cuturi. 2013. Sinkhorn Distances: Lightspeed Computation of Optimal Transport. In *Advances in Neural Information Processing Systems (NIPS)*, C. J. C. Burges, L. Bottou, M. Welling, Z. Ghahramani, and K. Q. Weinberger (Eds.), Vol. 26. Curran Associates, Inc. <https://proceedings.neurips.cc/paper/2013/file/af21d0c97db2e27e13572cbf59eb343d-Paper.pdf>
- [10] Mostafa Dehghani, Stephan Gouws, Oriol Vinyals, Jakob Uszkoreit, and Lukasz Kaiser. 2019. Universal Transformers. In *International Conference on Learning Representations*. <https://openreview.net/forum?id=HyzdRiR9Y7>
- [11] D. DeTone, T. Malisiewicz, and A. Rabinovich. 2018. SuperPoint: Self-supervised interest point detection and description. In *Proceedings of IEEE Conference on Computer Vision and Pattern Recognition Workshops (CVPRW)*. 337–33712.
- [12] M. Dusmanu, I. Rocco, T. Pajdla, M. Pollefeys, J. Sivic, A. Torii, and T. Sattler. 2019. D2-Net: A trainable CNN for joint description and detection of local features. In *Proceedings of IEEE Conference on Computer Vision and Pattern Recognition (CVPR)*. 8084–8093.
- [13] M. Fey, J. E. Lenssen, C. Morris, J. Masci, and N. M. Kriege. 2020. Deep Graph Matching Consensus. In *ICLR*.
- [14] Martin A. Fischler and Robert C. Bolles. 1981. Random Sample Consensus: A Paradigm for Model Fitting with Applications to Image Analysis and Automated Cartography. *Commun. ACM* 24, 6 (jun 1981), 381–395. <https://doi.org/10.1145/358669.358692>
- [15] Donniell E. Fishkind, Sancar Adali, Heather G. Patsolic, Lingyao Meng, Digvijay Singh, Vince Lyzinski, and Carey E. Priebe. 2019. Seeded graph matching. *Pattern Recognition* 87 (2019), 203–215. <https://doi.org/10.1016/j.patcog.2018.09.014>
- [16] Catherine Fraikin and Paul Van Dooren. 2007. Graph matching with type constraints on nodes and edges. In *Web Information Retrieval and Linear Algebra Algorithms (Dagstuhl Seminar Proceedings, 07071)*, Andreas Frommer, Michael W. Mahoney, and Daniel B. Szyld (Eds.). Internationales Begegnungs- und Forschungszentrum für Informatik (IBFI), Schloss Dagstuhl, Germany, Dagstuhl, Germany. <http://drops.dagstuhl.de/opus/volltexte/2007/1071>
- [17] J. Heinly, J. L. Schönberger, E. Dunn, and J. Frahm. 2015. Reconstructing the world\* in six days. In *Proceedings of IEEE Conference on Computer Vision and Pattern Recognition (CVPR)*. 3287–3295.
- [18] A. Katharopoulos, A. Vyas, N. Pappas, and F. Fleuret. 2020. Transformers are RNNs: Fast Autoregressive Transformers with Linear Attention. In *Proceedings of the International Conference on Machine Learning (ICML)*. <https://arxiv.org/abs/2006.16236>
- [19] Nikita Kitaev, Lukasz Kaiser, and Anselm Levskaya. 2020. Reformer: The Efficient Transformer. In *International Conference on Learning Representations*. <https://openreview.net/forum?id=rkgNKkHtvB>
- [20] Paul Knopp and Richard Sinkhorn. 1967. Concerning nonnegative matrices and doubly stochastic matrices. *Pacific J. Math.* 21, 2 (1967), 343 – 348. <https://doi.org/pjm/1102992505>
- [21] M. Leordeanu and M. Hebert. 2005. A spectral technique for correspondence problems using pairwise constraints. In *Tenth IEEE International Conference on Computer Vision (ICCV'05) Volume 1*, Vol. 2. 1482–1489 Vol. 2. <https://doi.org/10.1109/ICCV.2005.20>
- [22] Xinghui Li, Kai Han, Shuda Li, and Victor Prisacariu. 2020. Dual-Resolution Correspondence Networks. In *Conference on Neural Information Processing Systems (NeurIPS)*.
- [23] Zhengqi Li and Noah Snavely. 2018. MegaDepth: Learning Single-View Depth Prediction from Internet Photos. In *Proceedings of IEEE Conference on Computer Vision and Pattern Recognition (CVPR)*.
- [24] Philipp Lindenberger, Paul-Edouard Sarlin, Viktor Larsson, and Marc Pollefeys. 2021. Pixel-Perfect Structure-from-Motion with Featuremetric Refinement. In *International Conference on Computer Vision (ICCV)*.
- [25] Eliane Maria Loliola, Nair Maria Maia de Abreu, Paulo Oswaldo Boaventura-Netto, Peter Hahn, and Tania Querido. 2007. A survey for the quadratic assignment problem. *European Journal of Operational Research* 176, 2 (2007), 657–690. <https://doi.org/10.1016/j.ejor.2005.09.032>
- [26] David G. Lowe. 2004. Distinctive Image Features from Scale-Invariant Keypoints. *Int. J. Comput. Vision* 60, 2 (nov 2004), 91–110. <https://doi.org/10.1023/B:VISI.0000029664.99615.94>
- [27] Z. Luo, L. Zhou, X. Bai, H. Chen, J. Zhang, Y. Yao, S. Li, T. Fang, and L. Quan. 2020. ASLFeat: Learning local features of accurate shape and localization. In *Proceedings of IEEE Conference on Computer Vision and Pattern Recognition (CVPR)*.
- [28] J. Ma, Xingyu Jiang, Aoxiang Fan, Junjun Jiang, and Junchi Yan. 2020. Image Matching from Handcrafted to Deep Features: A Survey. *International Journal of Computer Vision* 129 (2020), 23–79.
- [29] Niki J. Parmar, Ashish Vaswani, Jakob Uszkoreit, Lukasz Kaiser, Noam Shazeer, Alexander Ku, and Dustin Tran. 2018. Image Transformer. In *International Conference on Machine Learning (ICML)*. <http://proceedings.mlr.press/v80/parmar18a.html>
- [30] Gabriel Peyré and Marco Cuturi. 2019. *Computational Optimal Transport: With Applications to Data Science*.
- [31] Jack W. Rae, Anna Potapenko, Siddhant M. Jayakumar, Chloe Hillier, and Timothy P. Lillicrap. 2020. Compressive Transformers for Long-Range Sequence Modelling. In *International Conference on Learning Representations*. <https://openreview.net/forum?id=SyJKikSYDH>
- [32] Jerome Revaud, Philippe Weinzaepfel, César Roberto de Souza, and Martin Humenberger. 2019. R2D2: Repeatable and Reliable Detector and Descriptor. In *NeurIPS*.
- [33] I. Rocco, R. Arandjelović, and J. Sivic. 2017. Convolutional neural network architecture for geometric matching. In *Proceedings of IEEE Conference on Computer Vision and Pattern Recognition (CVPR)*.
- [34] I. Rocco, R. Arandjelović, and J. Sivic. 2020. Efficient Neighbourhood Consensus Networks via Submanifold Sparse Convolutions. In *Proceedings of the European Conference on Computer Vision (ECCV)*.
- [35] Michal Rolínek, Paul Swoboda, Dominik Zietlow, Anselm Paulus, Vít Musil, and Georg Martius. 2020. Deep Graph Matching via Blackbox Differentiation of Combinatorial Solvers. In *Proceedings of the European Conference on Computer Vision (ECCV)*.
- [36] Paul-Edouard Sarlin, Daniel DeTone, Tomasz Malisiewicz, and Andrew Rabinovich. 2020. SuperGlue: Learning Feature Matching With Graph Neural Networks. In *Proceedings of IEEE Conference on Computer Vision and Pattern Recognition (CVPR)*.
- [37] Torsten Sattler, Bastian Leibe, and Leif Kobbelt. 2009. SCRAMSAC: Improving RANSAC’s efficiency with a spatial consistency filter. In *2009 IEEE 12th International Conference on Computer Vision*. 2090–2097. <https://doi.org/10.1109/ICCV.2009.5459459>
- [38] T. Sattler, W. Maddern, C. Toft, A. Torii, L. Hammarstrand, E. Stenborg, D. Safari, M. Okutomi, M. Pollefeys, J. Sivic, F. Kahl, and T. Pajdla. 2018. Benchmarking 6DOF outdoor visual localization in changing conditions. In *Proceedings of IEEE Conference on Computer Vision and Pattern Recognition (CVPR)*. 4104–4113.
- [39] T. Sattler, A. Torii, J. Sivic, M. Pollefeys, H. Taira, M. Okutomi, and T. Pajdla. 2017. Are Large-Scale 3D models really necessary for accurate visual localization?. In *Proceedings of IEEE Conference on Computer Vision and Pattern Recognition (CVPR)*. 6175–6184.
- [40] T. Sattler, T. Weyand, B. Leibe, and L. Kobbelt. 2012. Image Retrieval for image-Based localization revisited. In *Proceedings of the British Machine Vision Conference*. BMVA Press, 76.1–76.12.
- [41] J. L. Schönberger and J. Frahm. 2016. Structure-from-Motion revisited. In *Proceedings of IEEE Conference on Computer Vision and Pattern Recognition (CVPR)*. 4104–4113.
- [42] J. L. Schönberger, H. Hardmeier, T. Sattler, and M. Pollefeys. 2017. Comparative evaluation of hand-crafted and learned local Features. In *Proceedings of IEEE Conference on Computer Vision and Pattern Recognition (CVPR)*. 6959–6968.
- [43] Zhuoran Shen, Mingyuan Zhang, Haiyu Zhao, Shuai Yi, and Hongsheng Li. 2021. Efficient Attention: Attention With Linear Complexities. In *Proceedings of the IEEE/CVF Winter Conference on Applications of Computer Vision (WACV)*.
- [44] Jiaming Sun, Zehong Shen, Yuang Wang, Hujun Bao, and Xiaowei Zhou. 2021. LoFTR: Detector-Free Local Feature Matching with Transformers. *Proceedings of IEEE Conference on Computer Vision and Pattern Recognition (CVPR)*.

- [45] Paul Swoboda, Jan Kuske, and Bogdan Savchynskyy. 2017. A Dual Ascent Framework for Lagrangean Decomposition of Combinatorial Problems. In *Proceedings of IEEE Conference on Computer Vision and Pattern Recognition (CVPR)*. 4950–4960. <https://doi.org/10.1109/CVPR.2017.526>
- [46] Lorenzo Torresani, Vladimir Kolmogorov, and Carsten Rother. 2008. Feature Correspondence Via Graph Matching: Models and Global Optimization. In *Proceedings of the European Conference on Computer Vision (ECCV)*. Springer Berlin Heidelberg, 596–609.
- [47] Lorenzo Torresani, Vladimir Kolmogorov, and Carsten Rother. 2013. A Dual Decomposition Approach to Feature Correspondence. *IEEE Transactions on Pattern Analysis and Machine Intelligence* 35, 2 (2013), 259–271. <https://doi.org/10.1109/TPAMI.2012.105>
- [48] Nikolai Ufer and Björn Ommer. 2017. Deep Semantic Feature Matching. In *Proceedings of IEEE Conference on Computer Vision and Pattern Recognition (CVPR)*. 5929–5938. <https://doi.org/10.1109/CVPR.2017.628>
- [49] Ashish Vaswani, Noam Shazeer, Niki Parmar, Jakob Uszkoreit, Llion Jones, Aidan N Gomez, Łukasz Kaiser, and Illia Polosukhin. 2017. Attention is All you Need. In *Advances in Neural Information Processing Systems*, I. Guyon, U. V. Luxburg, S. Bengio, H. Wallach, R. Fergus, S. Vishwanathan, and R. Garnett (Eds.), Vol. 30. Curran Associates, Inc. <https://proceedings.neurips.cc/paper/2017/file/3f5ee243547dee91fbd053c1c4a845aa-Paper.pdf>
- [50] Cédric Villani. 2008. Optimal Transport: Old and New.
- [51] Sinong Wang, Belinda Z. Li, Madian Khabsa, Han Fang, and Hao Ma. 2020. Linformer: Self-Attention with Linear Complexity. [arXiv:2006.04768](https://arxiv.org/abs/2006.04768)
- [52] Zihao Wang, Xueyi Li, and Zhen Li. 2021. Local Representation is Not Enough: Soft Point-Wise Transformer for Descriptor and Detector of Local Features. In *Proceedings of the Thirtieth International Joint Conference on Artificial Intelligence, IJCAI-21*, Zhi-Hua Zhou (Ed.). International Joint Conferences on Artificial Intelligence Organization, 1150–1156. Main Track.
- [53] Andrei Zanfir and Cristian Sminchisescu. 2018. Deep Learning of Graph Matching. In *Proceedings of IEEE Conference on Computer Vision and Pattern Recognition (CVPR)*. 2684–2693. <https://doi.org/10.1109/CVPR.2018.00284>
- [54] Jiahui Zhang, Dawei Sun, Zixin Luo, Anbang Yao, Lei Zhou, Tianwei Shen, Yurong Chen, Long Quan, and Hongen Liao. 2019. Learning Two-View Correspondences and Geometry Using Order-Aware Network. In *International Conference on Computer Vision (ICCV)*.
- [55] Qunjie Zhou, Torsten Sattler, and Laura Leal-Taixe. 2021. Patch2Pix: Epipolar-Guided Pixel-Level Correspondences. In *Proceedings of IEEE Conference on Computer Vision and Pattern Recognition (CVPR)*.

## A Parameter settings

In the first layer, we set  $W'_Q$ ,  $W'_K$ , and  $W'_V$  to linearly project from high to low dimensional space. Given that the dimensionality of SuperPoint is 256, the linear projection maps from  $256 \rightarrow 64$ , and for any subsequent layer,  $D$ ,  $D_Q$ ,  $D_K$ ,  $D_V = 64$ . The encoded descriptors with 64 dimensions are reshaped to  $8 \times 8$  for multi-head attention (the number of heads = 8). For the local neighborhood selection, we set  $\theta = 1.0$  for Lowe’s Thresholding. For Eq. (10), we use  $\lambda = 2$  for image matching and 3D reconstruction and  $\lambda = 3$  for localization, where  $\mathcal{R}$ ,  $\mathcal{R}_s$ ,  $\mathcal{R}_t = \sqrt{\frac{H \times W}{100\pi}}$ .

## B Training datasets

We train the proposed model with Megadepth [23] datasets using the same image scenes as [36]. For each epoch, we sample 100 pairs per scene and select the pair with overlapping scores in range [0.5, 1]. Given an image pair, we extract the local features using SuperPoint [11] and sample 1024 keypoints per image. To generate the ground truth correspondence, we use the camera poses with depth maps corresponding to the two images to project the keypoints. The reprojection distances of the keypoints is used to determine ground truth matches and unmatchable points. Following [36], a pair of keypoints are considered ground truth matches if they are mutual nearest with a reprojection distance lower than 3 pixels; otherwise, it is labeled as unmatchable. We further filter out pairs if the ground truth matches are fewer than 50. Our data generation produces around 200k training pairs in total.

**Table 10: Sinkhorn vs. distance matching and filtering on #matches and inlier ratio.**

Methods	#Matches	InL.Ratio
SuperPoint + SuperGlue [36]	$8.32 \times 10^2$	<b>0.84</b>
SuperPoint + Our Linear. + Sink-100	$6.67 \times 10^2$	0.76
SuperPoint + Our Linear. + Dist.Match. + Filt.	$6.73 \times 10^2$	<b>0.82</b>

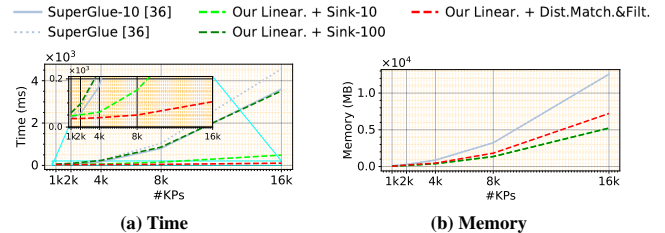


**Figure 7: Comparison on (a) time and (b) memory cost.**

**Learning.** We use Adam optimizer with learning rate of  $10^{-3}$  with exponential decay rate of 0.99992. We train for 10 epochs.

## C Evaluation protocols & settings

### C.1 3D Reconstruction

Exhaustive matching that matches the global information between all possible images is used to retrieve images for the small datasets, Herzjesu and Fountain. Meanwhile, NetVLAD [2] is used to retrieve the top 20 nearby images from South-Building, Madrid Metropolis, Gendarmenmarkt, and Tower of London. Sparse and dense reconstruction are performed by the SfM and MVS from COLMAP [41].

### C.2 Visual Localization

According to the protocols of *Visual Localization Benchmark\**, we provided the costumed features and performed image registration with COLMAP [41]; then, the localization is performed. We use the Aachen Day-Night datasets [38, 40] whose goal is to match images with extreme day-night changes for 98 queries.

## D Sinkhorn vs. Distance Matching & Filtering

Table 10 provides the comparison between using Sinkhorn versus distance matching & filtering with the linear transformer. Following [36], we have trained the linear transformer with Sinkhorn with optimal transport loss (similar settings to Section B). Using Sinkhorn does not provide higher #matches nor inlier ratios, yet Sinkhorn requires much higher time cost in Fig. 7.

## E Additional Ablation Studies

In this section, we provide the additional results to confirm our conclusion in Section 4.1. We provide the results of the localization accuracy across all the three error tolerances, *i.e.*, (0.25m,  $2^\circ$ ), (0.5m,  $5^\circ$ ), (5m,  $10^\circ$ ) on Aachen Day-Night [38, 40].

### E.1 Components in the Proposed Network.

Table 11 demonstrates the impact of components in the proposed network (Fig. 4) on the localization accuracy across all the three error tolerances. Our *Pair.Neigh. (No Filt.)*, without any filtering process,

\* <https://www.visuallocalization.net/>

**Table 11: Impact of components in the proposed network (Fig. 4) on localization accuracy.**

No. Methods	Network Architecture						Accuracy @ 0.25m, 2°				Accuracy @ 0.5m, 5°				Accuracy @ 5m, 10°			
	LA	PA	DM	Filt.	#dim	size	1k	2k	3k	4k	1k	2k	3k	4k	1k	2k	3k	4k
1 AdaLAM [4]	-	-	✓	✓	256	-	41.8	71.4	<b>79.6</b>	76.5	52.0	80.6	85.7	<b>86.7</b>	61.2	87.8	<b>92.9</b>	95.9
2 Our <i>Linear.</i> (No Filt.)	$L_1=10$	✗	✓	✗	64	S	<b>61.2</b>	<b>72.4</b>	73.5	76.5	<b>71.4</b>	81.6	81.6	<b>87.8</b>	<b>75.5</b>	87.8	91.8	95.9
3 Our <i>Pair.Neigh.</i> (No Filt.)	$L_1=8$	$L_2=2$	✓	✗	64	S	<b>66.3</b>	<b>74.5</b>	73.5	76.5	<b>74.5</b>	<b>83.7</b>	83.7	83.7	<b>82.7</b>	91.8	<b>93.9</b>	93.9
4 Our <i>Linear.</i>	$L_1=10$	✗	✓	✓	64	S	48.0	<b>73.5</b>	76.5	77.6	59.2	<b>82.7</b>	84.7	84.7	64.3	90.8	<b>92.9</b>	<b>98.9</b>
5 Our <i>Pair.Neigh.</i>	$L_1=8$	$L_2=2$	✓	✓	64	S	<b>58.2</b>	<b>72.4</b>	<b>78.6</b>	<b>80.6</b>	<b>65.3</b>	<b>85.7</b>	<b>86.7</b>	<b>86.7</b>	<b>73.5</b>	<b>93.9</b>	<b>95.9</b>	95.9
6 Our <i>Pair.Neigh.</i> -L	$L_1=8$	$L_2=2$	✓	✓	256	L	<b>63.3</b>	<b>73.5</b>	74.5	<b>78.6</b>	<b>70.4</b>	<b>85.7</b>	<b>87.8</b>	<b>87.8</b>	<b>76.5</b>	<b>94.9</b>	<b>95.9</b>	<b>96.9</b>

LA: Linear Attention layer, PN: Pairwise Neighborhood Attention layer, DM: Distance Matching, Filt: Filtering process, #dim: Encoded feature dimension, C', size: Network size, large (L) or small (S).

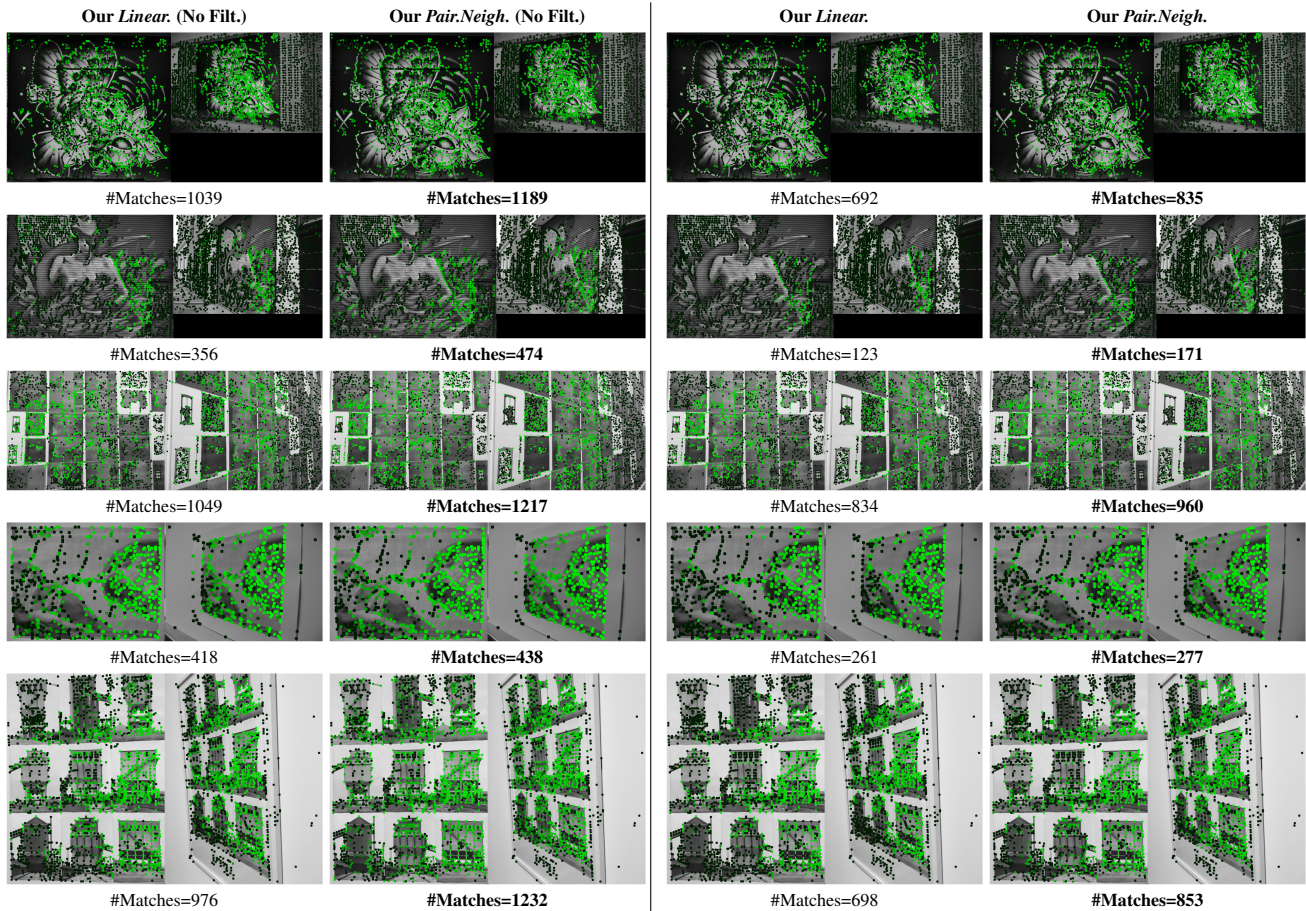


**Figure 8: The impact of pairwise neighborhood attention and linear attention layers on keypoint matching. We provide the keypoint matching samples by our *Linear.*, *Linear.* (No Filt.), *Pair.Neigh.*, and *Pair.Neigh.* (No Filt.). Our *Pair.Neigh.* and *Pair.Neigh.* (No Filt.) can match more and cover more areas than *Linear.* and *Linear.* (No Filt.) that uses only linear attention layers.**

offers higher accuracy than *Linear.* when the number of keypoints is low. This could be due to the combination of pairwise neighborhood (PN) and linear attention (LA). Meanwhile, our *Linear.* uses the linear attention layers only. Employing the filtering process (Filt) can improve the performance further, yet the performance gain is more obvious with *Pair.Neigh.*. The large-size model (*Pair.Neigh.*-L)

provides the highest accuracy in most cases. Fig. 8 demonstrates the combination of pairwise neighborhood and linear attention layers versus using linear attention layers only on the keypoint matching. We provide the output samples of keypoint matching resulted from our *Linear.* (No Filt.), *Pair.Neigh.* (No Filt.), and *Linear.* and *Pair.Neigh.*. The matched keypoints are highlighted with the green,



**Table 12: Impact of configurations in Local Neighborhood Selection (Section 3.4) on Localization Accuracy.**

No. Methods	Local Neigh. Selection		Accuracy @ 0.25m, 2°				Accuracy @ 0.5m, 5°				Accuracy @ 5m, 10°			
	Input	Seed Sep. Eq. (9)	1k	2k	3k	4k	1k	2k	3k	4k	1k	2k	3k	4k
1 Our <i>Pair.-w/oSep-Inp.</i>	$x^s, x^t$	✗	<u>59.2</u>	<u>75.5</u>	<u>74.5</u>	77.6	<u>69.4</u>	<u>84.7</u>	<u>84.7</u>	<u>84.7</u>	<u>75.5</u>	<u>93.9</u>	<u>94.9</u>	<u>94.9</u>
2 Our <i>Pair.-w/oSep.</i>	$\hat{f}^s, \hat{f}^t$	✗	57.1	71.4	<u>74.5</u>	<u>78.6</u>	<u>65.3</u>	82.7	<u>86.7</u>	<u>86.7</u>	71.4	<u>93.9</u>	<u>94.9</u>	<u>95.9</u>
3 Our <i>Pair.Neigh.</i>	$\hat{f}^s, \hat{f}^t$	✓	<u>58.2</u>	<u>72.4</u>	<u>78.6</u>	<u>80.6</u>	<u>65.3</u>	<u>85.7</u>	<u>86.7</u>	<u>86.7</u>	<u>73.5</u>	<u>93.9</u>	<u>95.9</u>	<u>95.9</u>

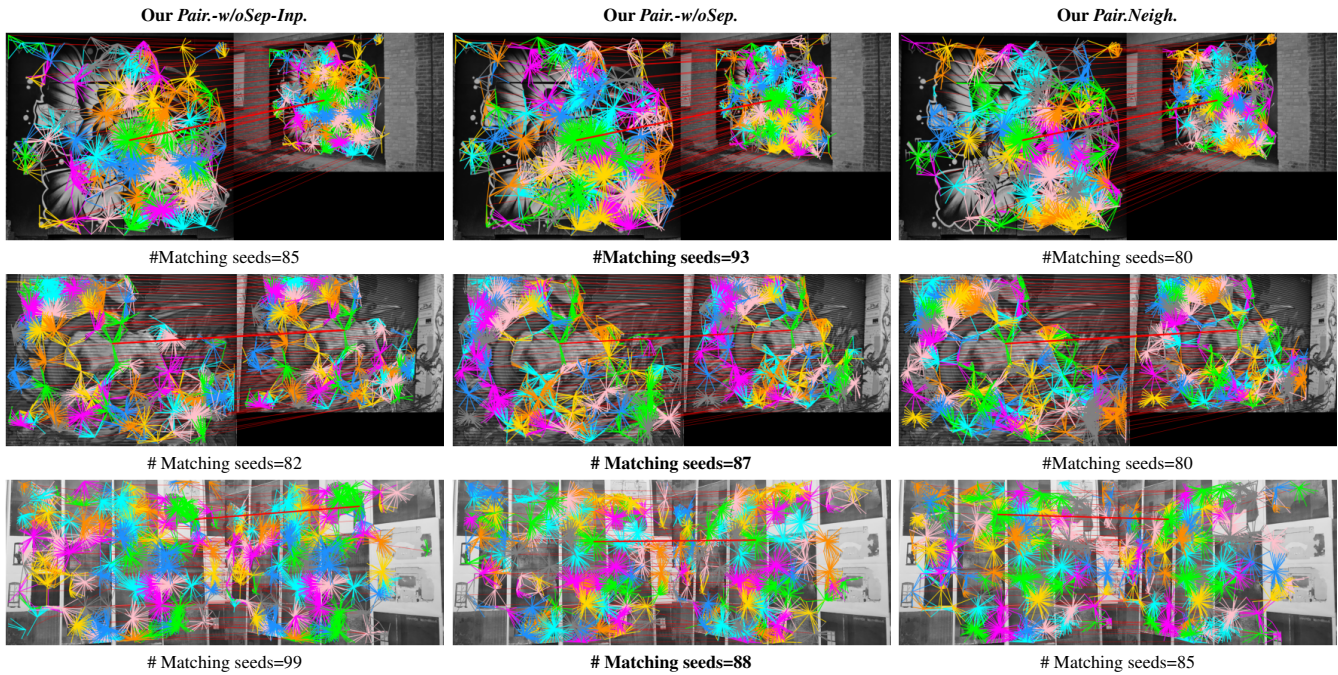


**Figure 9: The output samples from Local Neighborhood Selection (Section 3.4) configured according to our *Pair.-w/oSep-Inp.*, *Pair.-w/oSep.*, and *Pair.Neigh.* The local neighborhood selection of *Pair.-w/oSep-Inp.* depends on the input descriptors  $x^s, x^t$ . However, the local neighborhood selection of our *Pair.-w/oSep.* and *Pair.Neigh.* depends on  $\hat{f}^s, \hat{f}^t$ . Nevertheless, *Pair.-w/oSep.* ignores the separation condition; thus, it can collect more matching seeds than *Pair.Neigh.*.**

and the unmatched keypoints are in black. The brighter color indicates the higher similarity score between the encoded features from Transformers. Generally, *Pair.Neigh.* can match more keypoints and cover more areas than *Linear.*

## E.2 Local Neighborhood Selection.

Table 12 provides the impact on localization accuracy due to the configuration of Local Neighborhood Selection (Section 3.4). Our *Pair.-w/oSep-Inp.* offers higher robustness when number of keypoints are low. Meanwhile, *Pair.Neigh.* and *Pair.-w/oSep.* offer the highest accuracy when the number of keypoints are high, as  $\hat{f}^s, \hat{f}^t$  are resulted from the aggregation of information. Using both pairwise neighborhood attention and linear attention layers offers higher accuracy than using only linear attention layer in most cases.

Fig. 9 demonstrates the output samples from the Local Neighborhood Selection by our *Pair.-w/oSep-Inp.*, *Pair.-w/oSep.*, and *Pair.Neigh.* at 2k keypoints. The local neighborhood selection of *Pair.-w/oSep-Inp.* depends on the input descriptors  $x^s, x^t$ . Meanwhile, the local

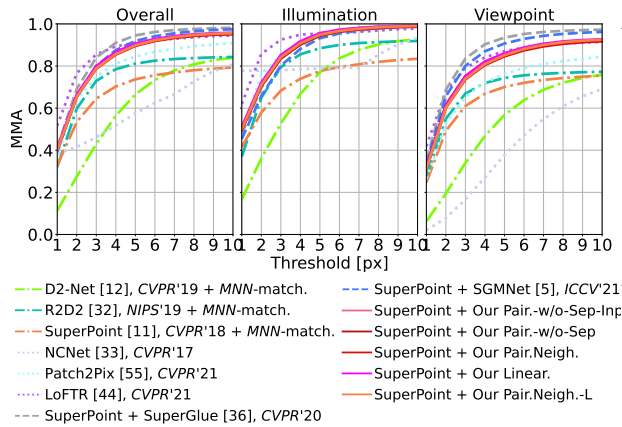
neighborhood selection of *Pair.-w/oSep.* and *Pair.Neigh.* depends on  $\hat{f}^s, \hat{f}^t$ . Since *Pair.-w/oSep.* ignores the separation condition, it can collect more matching seeds than *Pair.Neigh.* Despite having less matching seeds, *Pair.Neigh.* employs the seed separation condition which enforces the matching seeds to be spreading across the images. The spreading of matching seeds shows to be an important factor in gaining high accuracy in localization according to Table 12.

## F Additional SOTA Comparisons

This section provides the additional results of our work on *Linear.* and *Pair.Neigh.-L*, where Table 13 provides the summary of all the configuration and settings of our proposed method:

- Our *Linear.* Configuration No.4 in Table 13;
- Our *Pair.Neigh.-L* Configuration No.5 in Table 13.

The results are provided in the last two rows in addition to those results reported in the main paper, including our *Pair.Neigh.*, *Pair.-w/oSep-Inp.*, and *Pair.-w/oSep.*, which correspond to Configuration No.1, No.2, No.3 in Table 13. We compare with: • **Sparse matching:**



Methods	Pub.	#Matches	Inl.Ratio	#Param.	Total Time(ms) <sup>‡</sup>
D2-Net [12] + MNN-matching	CVPR'19	$2.50 \times 10^3$	0.42	$7.64 \times 10^6$	487.06
R2D2 [32] + MNN-matching	NIPS'19	$2.05 \times 10^3$	0.74	$1.04 \times 10^6$	1755.16
SuperPoint [11] + MNN-matching	CVPR'18	$1.08 \times 10^3$	0.65	$1.30 \times 10^6$	<b>34.30</b>
NCNet [33]	CVPR'17	$1.48 \times 10^3$	0.46	$21.3 \times 10^6$	297.18
Patch2Pix [55]	CVPR'21	$1.26 \times 10^3$	0.76	$31.6 \times 10^6$	453.07
LoFTR [44]	CVPR'21	<b><math>4.71 \times 10^3</math></b>	<b>0.87</b>	$11.6 \times 10^6$	212.98
SuperPoint + SuperGlue [36]	CVPR'20	$8.32 \times 10^2$	<b>0.84</b>	$12.0 \times 10^6$	115.14
SuperPoint + SGMNet [5]	ICCV'21	$8.66 \times 10^2$	0.80	$31.1 \times 10^6$	116.11
SuperPoint + Our Pair.-w/o-Sep-Inp.	—	$7.15 \times 10^2$	0.80	<b><math>0.841 \times 10^6</math></b>	<b>68.49</b>
SuperPoint + Our Pair.-w/o-Sep.	—	$6.97 \times 10^2$	<b>0.81</b>	<b><math>0.841 \times 10^6</math></b>	<b>68.58</b>
SuperPoint + Our Pair.Neigh.	—	$7.11 \times 10^2$	0.80	<b><math>0.841 \times 10^6</math></b>	73.52
SuperPoint + Our Linear.	—	$6.73 \times 10^2$	<b>0.82</b>	<b><math>0.924 \times 10^6</math></b>	73.60
SuperPoint + Our Pair.Neigh.-L	—	$7.19 \times 10^2$	0.80	$12.5 \times 10^6$	88.64

<sup>‡</sup> Total Time = Feature Extraction Time + Sparse/Dense Matching Time.

Figure 10: Image matching. Our method versus SOTAs — local features, dense matching, and sparse matching — on HPatches [3].

Table 13: Summary of the settings & configurations.

No.	Name	Network Architecture				Local Neigh. Sel.			
		LA	PA	DM Filtr.	#dim size	Inp.	Sep. Eq. (9)		
1	Our Pair.-w/oSep-Inp.	$L_1=8$	$L_2=2$	✓	✓	64	S	$x^s, x^t$	✗
2	Our Pair.-w/oSep.	$L_1=8$	$L_2=2$	✓	✓	64	S	$f^s, f^t$	✗
3	Our Pair.Neigh.	$L_1=8$	$L_2=2$	✓	✓	64	S	$f^s, f^t$	✓
4	Our Linear.	$L_1=10$	✗	✓	✓	64	S	N/A	N/A
5	Our Pair.Neigh.-L	$L_1=8$	$L_2=2$	✓	✓	256	L	$f^s, f^t$	✓

SuperGlue [36] and SGMNet [5]; • **Dense matching:** LoFTR [44], Patch2Pix [55], NCNet [33]; • **Local features:** SuperPoint [11], R2D2 [32], D2-Net [12], and ASLFeat [27], with the standard matching; • **Keypoint filtering:** AdaLAM [4] and OANet [54].

## F.1 Image Matching & Visual Results

This section provides the additional numerical results of our *Linear.* and *Pair.Neigh.-L* and the visual results of our method (Our *Pair.Neigh.*) on image matching task on HPatches [3].

**Numerical Results.** From Fig. 10, *Linear.* and *Pair.Neigh.-L* offers similar MMA curve to the other configuration of our work, Our *Linear.* offers higher *Inl.Ratio*, but lower matches. Meanwhile, *Pair.Neigh.-L* offers higher matches, but also 10-20 ms more runtime than other configurations of our works.

**Visual Results.** Fig. 11 and Fig. 12 provide the selected visual results of image matching on illumination and viewpoint changes between our method (*Pair.Neigh.*) versus SuperGlue and SGMNet. The correct and incorrect matches are denoted with green and red color, respectively. From the results on illumination changes in Fig. 11, our method provides the highest MMA with less incorrect matches on the illumination changes, which corresponds to the results in Fig. 10. Meanwhile, on viewpoint changes in Fig. 12, our work provides the accurate matches, but it achieves slightly lower performance due to the lower number of matches.

## F.2 3D Reconstruction & Visual Results

This section we provide the additional numerical results of *Linear.* and *Pair.Neigh.-L* on 3D reconstruction using ETH small- and medium-size datasets [42]. We also provide the visual results of our *Pair.Neigh.* in comparison with the SOTAs, SuperGlue and SGMNet.

**Numerical Results.** Table 14 and Table 15 provide the results on the small-size datasets—Fountain, Herzjesu, and South-Building—and the medium-size datasets—Madrid Metropolis, Gendarmenmarkt, and Tower of London. From Table 14, our *Linear.* and *Pair.Neigh.-L* offer similar performance to the other configurations of our work, *i.e.*, long *Track. Len.*, lower *Reproj. Error*, and comparable *Dense Points* to SuperGlue and SGMNet, SuperGlue-10, SGMNet-10. Despite our *Pair.Neigh.-L* being a larger model, its *Match. Time* only slightly higher than the other configurations of our work, which is about **7 times** and **1.6 times faster** than SuperGlue-10 and SGMNet-10, respectively. From Table 15, our *Linear.* and *Pair.Neigh.-L* provide long *Track. Len.*, low *Reproj. Error*, and moderate *Dense Points*, in most cases. Both *Linear.* and *Pair.Neigh.-L* achieve these results with similar runtime to the other configurations of our work, which is lower than the runtime of SuperGlue-10 and SGMNet-10. That is, the *Match. Time* is about **3 times** and **twice faster** than SuperGlue-10 and SGMNet-10, due to the lower detected keypoints by SuperPoint.

**Visual Results** Fig. 13 and Fig. 14 provides the visual results of the 3D reconstruction on the small- and the medium-size datasets. From Fig. 13, our method (*Pair.Neigh.*) provides the best visual results, the lowest *Reproj. Error*, and the longest *Track. Len.* in most cases. Here, we enlarged the 3D point clouds for Fountain and Herzjesu, and we applied the error threshold of 1.2 in all cases. On Fountain, our method provides similar visual results to SuperGlue and SGMNet. On Herzjesu, our method can capture slightly more details. Meanwhile, our work can provide overall denser 3D reconstruction on South-Building. From Fig. 14, our *Pair.Neigh.* produces the 3D reconstruction with the least artifacts, the lowest *Reproj. Error*, and the longest *Track. Len.*, in most cases. For example, on Genkarkmentmarkt, our *Pair.Neigh.* can capture the most of landmark with accurate 3D reconstruction. Meanwhile, SuperGlue-10 produces

**Table 14: Small-size ETH. Our methods versus the official SuperGlue and SGMNet, Superglue-10 and SGMet-10.**

Datasets	Methods	Track. Len.	Reproj. Error	Sparse Points	Dense Points	Match.	Time(sec)
Herzjesu 8 images	SuperGlue [36] <sup>†</sup>	4.45	0.921	<b>8.5k</b>	1.14M	$4.71 \times 10^2$	
	SuperGlue-10 [36]	4.44	0.921	<b>8.5k</b>	<b>1.15M</b>	$2.68 \times 10^2$	
	SGMNet [5] <sup>§</sup>	4.16	0.960	<b>9.6k</b>	1.14M	$1.43 \times 10^2$	
	SGMNet-10 [5]	4.14	0.955	<b>9.8k</b>	1.14M	$0.66 \times 10^2$	
	Our <i>Pair.-w/oSep-Inp.</i>	<b>4.54</b>	0.881	7.3k	1.14M	$0.24 \times 10^2$	
	Our <i>Pair.-w/oSep.</i>	<b>4.54</b>	<b>0.872</b>	7.2k	<b>1.15M</b>	$0.24 \times 10^2$	
	Our <i>Pair.Neigh.</i>	<b>4.53</b>	<b>0.873</b>	7.3k		$0.23 \times 10^2$	
	Our <i>Linear.</i>	4.52	<b>0.857</b>	7.1k	<b>1.15M</b>	$0.23 \times 10^2$	
	Our <i>Pair.Neigh.-L</i>	<b>4.53</b>	0.877	7.3k	<b>1.15M</b>	$0.39 \times 10^2$	
Fountain 11 images	SuperGlue [36] <sup>†</sup>	5.14	0.961	<b>11.4k</b>	<b>1.84M</b>	$7.90 \times 10^2$	
	SuperGlue-10 [36]	5.14	0.960	<b>11.4k</b>	1.83M	$4.42 \times 10^2$	
	SGMNet [5] <sup>§</sup>	4.93	0.959	<b>11.9k</b>	<b>1.84M</b>	$2.38 \times 10^2$	
	SGMNet-10 [5]	4.92	0.966	<b>11.9k</b>	<b>1.84M</b>	$1.12 \times 10^2$	
	Our <i>Pair.-w/oSep-Inp.</i>	<b>5.17</b>	0.909	10.0k	1.83M	$0.41 \times 10^2$	
	Our <i>Pair.-w/oSep.</i>	<b>5.16</b>	0.905	10.0k	1.83M	$0.42 \times 10^2$	
	Our <i>Pair.Neigh.</i>	<b>5.14</b>	<b>0.903</b>	10.0k	1.83M	$0.41 \times 10^2$	
	Our <i>Linear.</i>	5.12	<b>0.890</b>	9.8k	1.83M	$0.43 \times 10^2$	
	Our <i>Pair.Neigh.-L</i>	5.12	<b>0.901</b>	10.0k	1.83M	$0.71 \times 10^2$	
South-Building 128 images	SuperGlue [36] <sup>†</sup>	7.90	0.947	114.4k	<b>12.53M</b>	$402.23 \times 10^2$	
	SuperGlue-10 [36]	7.88	0.949	<b>114.8k</b>	<b>12.51M</b>	$228.43 \times 10^2$	
	SGMNet [5] <sup>§</sup>	6.95	0.979	<b>132.2k</b>	12.39M	$108.67 \times 10^2$	
	SGMNet-10 [5]	6.97	0.981	<b>131.2k</b>	12.33M	$48.79 \times 10^2$	
	Our <i>Pair.-w/oSep-Inp.</i>	<b>8.31</b>	0.837	94.8k	12.40M	$14.83 \times 10^2$	
	Our <i>Pair.-w/oSep.</i>	<b>8.31</b>	<b>0.832</b>	94.2k	12.42M	$13.86 \times 10^2$	
	Our <i>Pair.Neigh.</i>	8.27	<b>0.836</b>	95.1k	<b>12.45M</b>	$13.29 \times 10^2$	
	Our <i>Linear.</i>	<b>8.32</b>	<b>0.820</b>	92.2k	12.38M	$14.43 \times 10^2$	
	Our <i>Pair.Neigh.-L</i>	8.24	0.841	96.1k	12.43M	$27.71 \times 10^2$	

<sup>†</sup> SuperGlue with its official setting (Sinkhorn iter. = 100).

<sup>§</sup> SGMNet with its official setting (Sinkhorn iter. = 100, num. seeds = 128).

small inaccurate 3D point clouds in front of the concert hall between the two churches. SGMNet-10 produces the inaccurate 3D point clouds of the entire concert hall building. On Madrid Metropolis, our 3D reconstruction accurately captures the landmark but is more sparse than SuperGlue-10. Meanwhile, SGMNet-10 provides the inaccurate 3D point clouds on the opposite side to the Metropolis Building. However, on Tower of London, all of the methods struggle to provide the accurate result. Our 3D reconstruction is very sparse and misses parts of the castle on the tops. Meanwhile, SuperGlue and SGMNet produce many artifacts around the castle areas. This suggests the future improvement to maintain high accuracy.

### F.3 Visual Localization

This section we provide the additional numerical results of our *Linear.* on visual localization in Table 16. Our *Linear.* offers lower performance than the other configurations of our work—*Pair.-w/oSep-Inp.*, *Pair.-w/oSep.*, and *Pair.Neigh.*. This is because *Linear.* tends to provide the lower number of matches as shown in Figure 8 and Figure 10. On the other hand, our work such as our *Pair.Neigh.* provides the better localization accuracy as it offers the higher number of accurate matches. Although our *Pair.Neigh.* does not match as much as the SOTAs, SuperGlue and SGMNet, it offers better 3D

**Table 15: Medium-size ETH. Our method versus MNN+Lowe's Thresholding, AdaLAM, Superglue-10, and SGMNet-10.**

Datasets	Methods	Track. Len.	Reproj. Error	#Reg. Img.	Dense Points	Match. Time (H:M:S)
Madrid Metropolis 1344 images	MNN+Lowe's.(baseline) [26]	7.28	<b>1.066</b>	513	2.95M	<b>00:04:51</b>
	AdaLAM [4]	8.29	1.113	519	<b>3.04M</b>	<b>00:10:44</b>
	SuperGlue-10 [36]	7.59	1.240	<b>732</b>	<b>3.39M</b>	05:15:30
	SGMNet-10 [5]	6.99	1.211	<b>759</b>	<b>3.44M</b>	05:27:46
	Our <i>Pair.-w/oSep-Inp.</i>	8.19	<b>1.106</b>	<b>563</b>	2.54M	01:16:21
	Our <i>Pair.-w/oSep.</i>	<b>8.67</b>	1.114	508	2.88M	02:40:49
	Our <i>Pair.Neigh.</i>	<b>8.51</b>	1.118	523	3.02M	01:22:36
	Our <i>Linear.</i>	8.26	<b>1.090</b>	552	2.94M	<b>01:08:09</b>
	Our <i>Pair.Neigh.-L</i>	<b>8.34</b>	1.111	562	2.98M	01:51:17
Gendarmenmarkt 1463 images	MNN+Lowe's.(baseline) [26]	6.57	<b>1.069</b>	1034	<b>7.12M</b>	<b>00:05:23</b>
	AdaLAM [4]	<b>8.05</b>	1.135	<b>1041</b>	6.77M	<b>00:20:43</b>
	SuperGlue-10 [36]	<b>8.36</b>	1.222	<b>1060</b>	<b>7.24M</b>	07:08:39
	SGMNet-10 [5]	7.53	1.203	<b>1124</b>	6.64M	05:12:59
	Our <i>Pair.-w/oSep-Inp.</i>	7.89	1.117	1039	7.00M	02:29:20
	Our <i>Pair.-w/oSep.</i>	7.91	<b>1.103</b>	1039	<b>7.06M</b>	02:56:32
	Our <i>Pair.Neigh.</i>	7.92	1.116	1030	6.96M	02:02:18
	Our <i>Linear.</i>	7.95	<b>1.101</b>	1027	7.00M	<b>01:57:50</b>
	Our <i>Pair.Neigh.-L</i>	<b>8.11</b>	1.134	1001	6.67M	02:45:46
Tower of London 1576 images	MNN+Lowe's.(baseline) [26]	7.44	<b>1.014</b>	733	5.09M	<b>00:05:49</b>
	AdaLAM [4]	8.46	1.044	777	5.47M	<b>00:13:28</b>
	SuperGlue-10 [36]	7.27	1.145	<b>941</b>	<b>5.97M</b>	06:22:13
	SGMNet-10 [5]	6.78	1.145	<b>879</b>	<b>5.66M</b>	05:02:00
	Our <i>Pair.-w/oSep-Inp.</i>	<b>8.51</b>	1.041	766	<b>5.53M</b>	02:17:24
	Our <i>Pair.-w/oSep.</i>	<b>8.63</b>	1.040	776	5.41M	03:19:36
	Our <i>Pair.Neigh.</i>	8.49	<b>1.038</b>	779	5.43M	01:46:00
	Our <i>Linear.</i>	<b>8.52</b>	<b>1.024</b>	<b>796</b>	5.50M	<b>01:21:16</b>
	Our <i>Pair.Neigh.-L</i>	8.49	1.046	768	5.45M	02:22:14

**Table 16: Visual localization on Aachen Day-Night.**

Methods	#kpts	#dim	#Param.	Cplx.	0.25m, 2°	0.5m, 5°	5m, 10°
D2-Net [12]	19K	512	15M	-	74.5	86.7	<b>100.0</b>
ASLFeat [27] v.2	10K	128	<b>0.4M</b>	-	<b>81.6</b>	87.8	<b>100.0</b>
R2D2 [32] $N = 8$	40K	128	1.0M	-	76.5	<b>90.8</b>	<b>100.0</b>
SPTD2 [52]	10K	128	-	-	78.8	<b>89.3</b>	<b>99.0</b>
SuperPoint [11] + SOTA Filtering/Matching							
↳ Baseline MNN	<b>4K</b>	256	-	-	71.4	78.6	87.8
↳ OANet [4]	<b>4K</b>	256	4.8M	-	77.6	<b>90.8</b>	<b>100.0</b>
↳ AdaLAM [4]	<b>4K</b>	256	-	-	76.5	86.7	95.9
↳ SuperGlue [36]	<b>4K</b>	256	12M	$N^2C$	79.6	<b>90.8</b>	<b>100.0</b>
↳ SGMNet [5]	<b>4K</b>	256	31M	$NKC + K^2C$	77.6	88.8	<b>99.0</b>
↳ Our <i>Pair.-w/oSep-Inp.</i>	<b>4K</b>	<b>64</b>	<b>0.8M</b>	$\approx NC^2$	77.6	84.7	94.9
↳ Our <i>Pair.-w/oSep.</i>	<b>4K</b>	<b>64</b>	<b>0.8M</b>	$\approx NC^2$	78.6	86.7	95.9
↳ Our <i>Pair.Neigh.</i>	<b>4K</b>	<b>64</b>	<b>0.8M</b>	$\approx NC^2$	<b>80.6</b>	86.7	95.9
↳ Our <i>Linear.</i>	<b>4K</b>	<b>64</b>	<b>0.8M</b>	$\approx NC^2$	77.6	84.7	92.9
↳ Our <i>Pair.Neigh.-L</i>	<b>4K</b>	256	12M	$\approx NC^2$	78.6	87.8	96.9

reconstruction as shown in Table 14 and Table 15, leading to the better accuracy than the SOTAs.



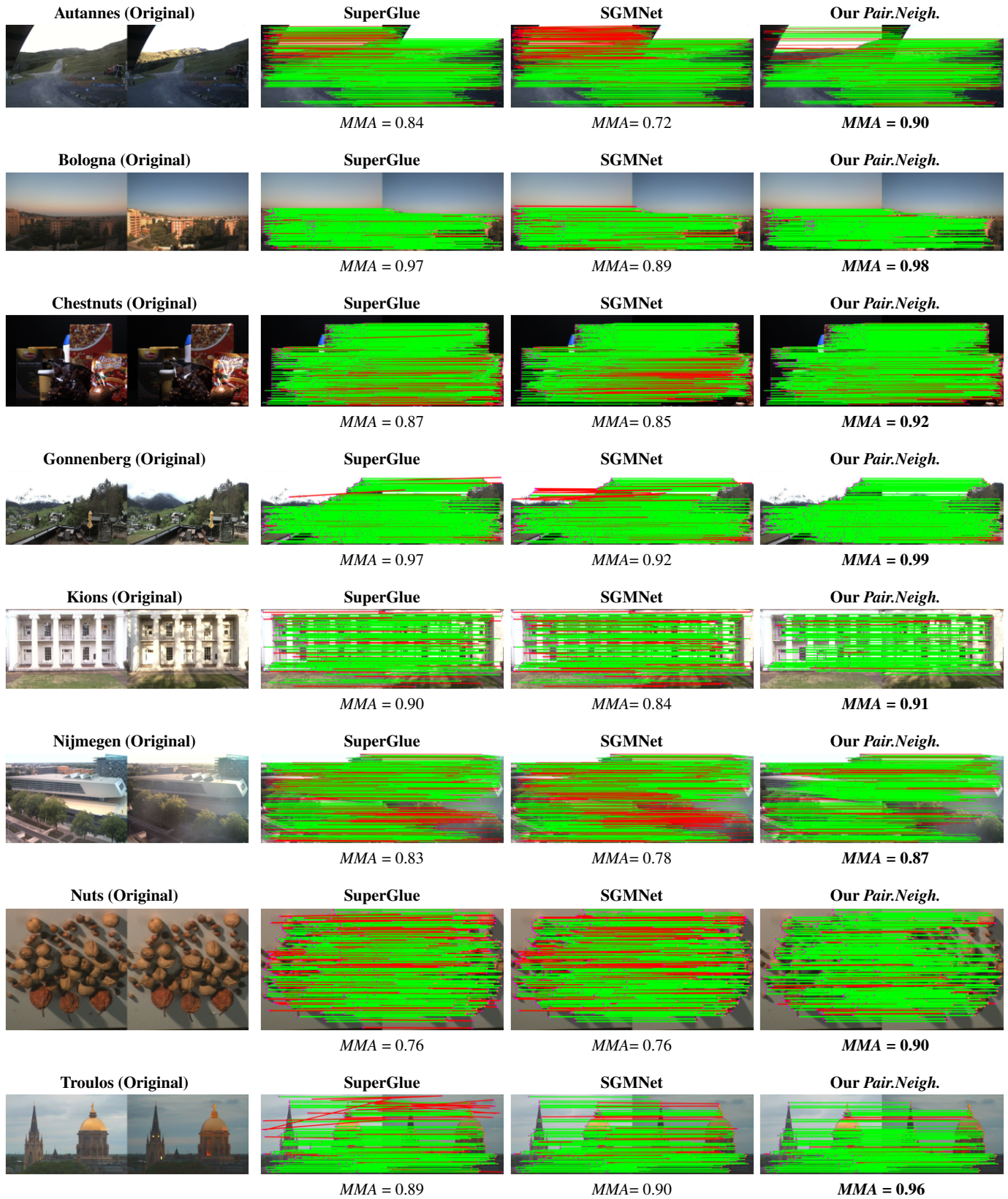


Figure 11: Image matching against illumination changes on HPatches by SuperGlue, SGMNet, and our Pair.Neigh.



Figure 12: Image matching against viewpoint changes on HPatches by SuperGlue, SGMNet, and Our Pair.Neigh.



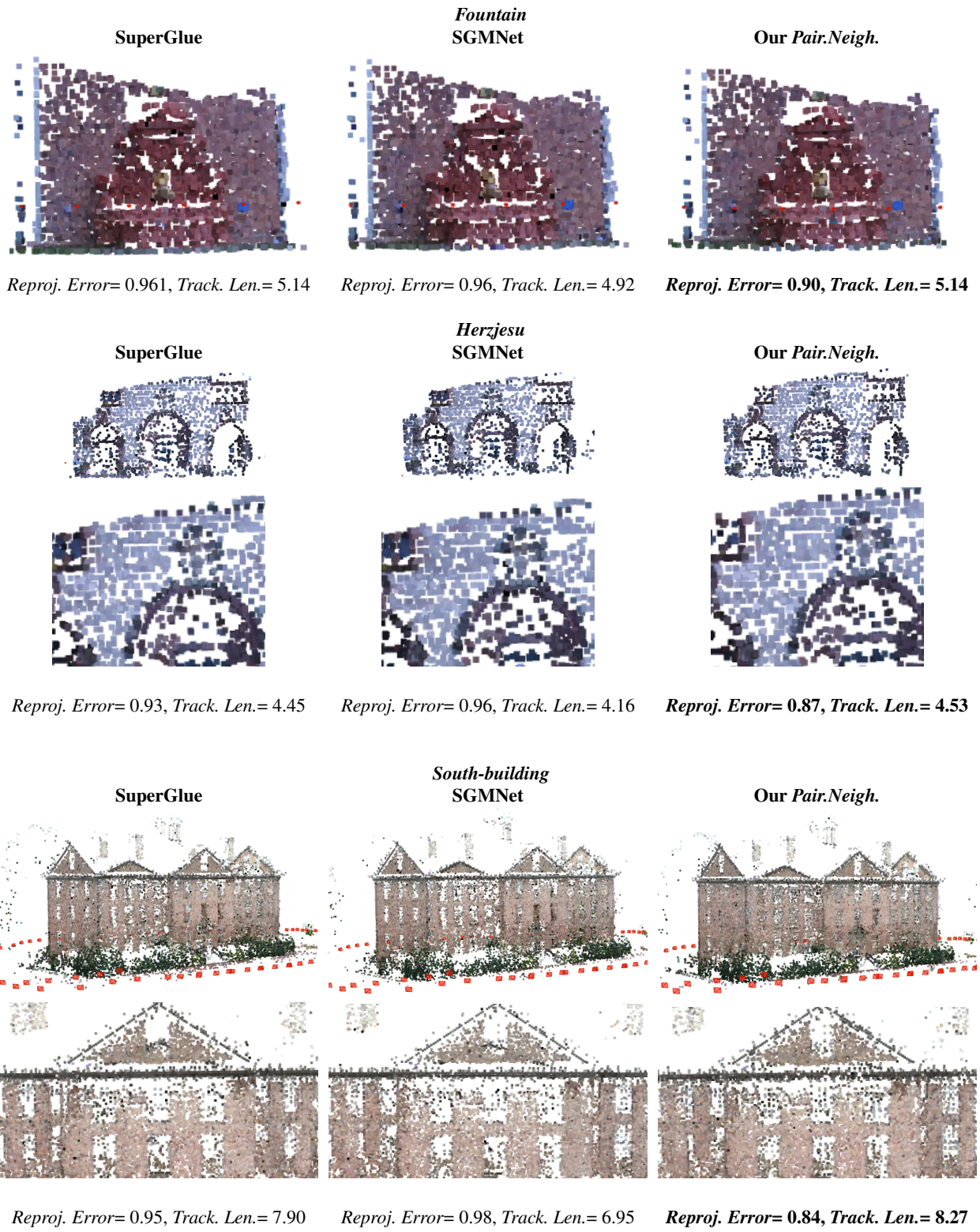
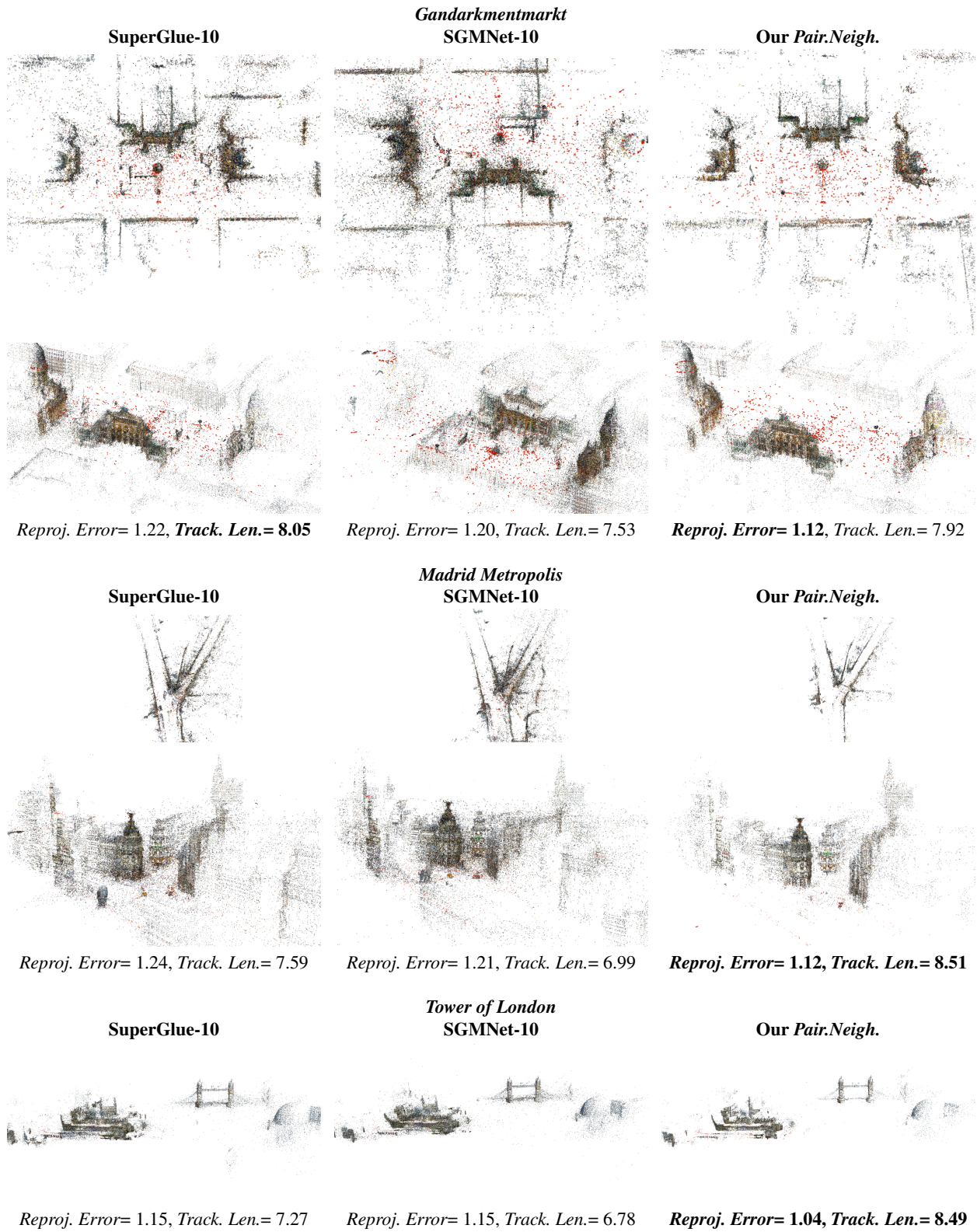


Figure 13: 3D Reconstruction on small-size datasets by SuperGlue (left), SGMNet (middle), and Our Pair.Neigh (right).





**Figure 14: 3D Reconstruction on medium-size datasets by SuperGlue (left), SGMNet (middle), and Our Pair.Neigh (right).**